V.S.Patsko, V.L.Turova

NUMERICAL STUDY OF DIFFERENTIAL GAMES WITH THE HOMICIDAL CHAUFFEUR DYNAMICS

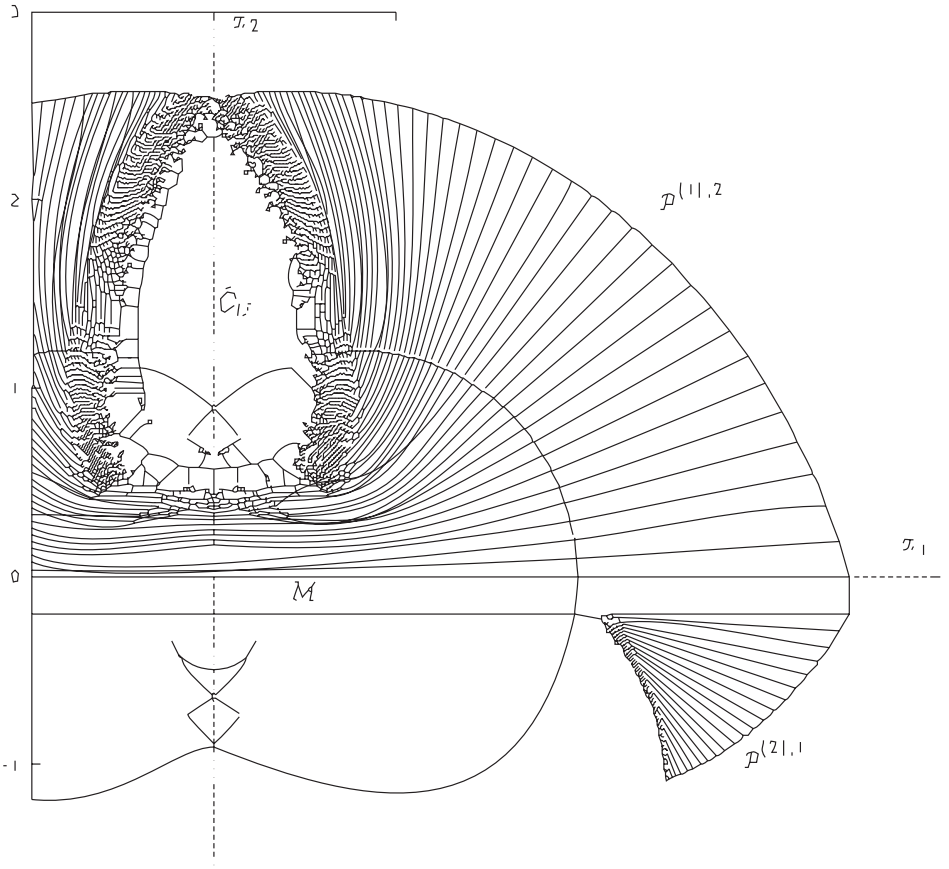

RUSSIAN ACADEMY OF SCIENCES
Ural Branch
Institute of Mathematics and Mechanics

Scientific reports

V.S.Patsko, V.L.Turova

NUMERICAL STUDY OF DIFFERENTIAL GAMES WITH THE HOMICIDAL CHAUFFEUR DYNAMICS

Ekaterinburg
2000

Approved and recommended for publication by
Scientific Board of the Institute of Mathematics and Mechanics
Ural Branch of RAS

Patsko V.S., Turova V.L.
Numerical study of differential games with the homicidal chauffeur dynamics: Scientific reports.
IMM Ural Branch of RAS. Ekaterinburg, Russia, 2000.

The dynamics of the homicidal chauffeur describes the pursuit of a non-inertial object by an inertial one. In the paper, three differential games with the homicidal chauffeur dynamics are studied: the classical Isaacs' homicidal chauffeur game, the acoustic version of Bernhard, and the surveillance-evasion game by Lewin and Olsder. Level sets of the value function are computed for these differential games. The computation is carried out using the algorithm based on the propagation of fronts. The structure of the value function is found to be very complicated. An explanation to peculiarities of the solutions is given based on the analysis of families of semipermeable curves. The paper can be of interest for specialists in the theory of optimal control and differential games. The computation results can serve as test examples for new algorithms that are developed for solving nonlinear differential games in the plane.

Illustr. 64, refs. 34.

Scientific reviewer V.N.Ushakov, Dr. of phys.-math.sci., Prof.

Abstract. Three differential games with the dynamics of the homicidal chauffeur are considered. The first problem is the Isaacs' homicidal chauffeur differential game. In this game, a pursuer P minimizes the capture time of an evader E. The objective of the evader is to prevent the capture or to maximize the capture time. The magnitude of the velocity is constant for the pursuer, and his maneuverability is bounded through a minimal turn radius. The maneuverability of the evader is not bounded. The pursuer's control is the rate of turn, the evader steers by choosing directions of his velocity. The main difference of the second problem is that the size of the constraint on the control parameter of the evader depends on the position of the game. The idea of such a modification was suggested by Bernhard. The third problem is a conic surveillance-evasion game studied by Lewin and Olsder. In this game, the dynamics is the same as in the Isaacs' problem but the aims of the players differ from the classic formulation: an evader E minimizes the time of escaping from a detection set which is a two-dimensional semi-infinite cone. The detection set is attached to the velocity vector of a pursuer P whose objective is to keep the evader within the detection set for maximal time. The paper describes the computation of level sets of the value functions for these games. An algorithm proposed by the authors is used. An analysis of families of semipermeable curves is carried out. The results of this analysis are used to check the correctness of the computation of level sets and to explain the appearance of holes in victory domains of the pursuer in the second problem.

Keywords: Differential games, time-optimal control, homicidal chauffeur game, value function, families of semipermeable curves, numerical algorithm, backward procedures

AMS classification: 90D25, 90D26, 49N55

Contents

1. Introduction

The homicidal chauffeur game was formulated more than thirty years ago in [15]. Since that time, many authors studied this problem in various ways. The most complete qualitative solution was given in [20].

In many papers (see, for example, [8], [10], [12], [18] and [19]), the problems with some alterations of the dynamics or objectives of the players were considered.

In [7], an acoustic version of the homicidal chauffeur problem was proposed. The evader must apply a reduced speed (in order not to be heard by the pursuer) when the distance between him and the pursuer becomes less than a given value. In [10] and [12] level sets of the value function for particular magnitudes of parameters of the problem were computed using an algorithm based on viability theory. The solution to the problem has a complicated structure: holes in the solvability set (in the victory domain) of the pursuer can arise, the evader being safe from the pursuer within these holes.

In [19], a surveillance-evasion game with the pursuer's detection zone in the shape of a cone was stated and a qualitative solution to this problem was given. Similar to [20], the space of parameters of the problem was divided into subregions. In each subregion, the type of solution (possible singular lines and the strategies of the players) was described.

In this paper, the homicidal chauffeur game in the classical statement of Isaacs and modified problems from [10] and [19] are studied using an algorithm proposed by the authors for computation of level sets of the value function. Our method is based on general theory of differential games (see [16] and [17]). The algorithm is a natural extension of the algorithms from [27] and exploits ideas of the algorithms from [23]–[25] for linear time-optimal differential games in the plane. Some experience (see [21]–[23], [27] and [32]) in solving differential games of kind [15] in the plane helps to find out very complicated types of solutions and to verify the solutions validity. The computation results are consistent with those obtained in [10], [19] and [20]. The algorithm uses specific properties of the plane and is very accurate. It allows to explore some fine peculiarities of the solutions. The development of such algorithms together with the general algorithms from [3]–[5], [9], [10], [12], [13], [14], [28]–[31], [33] and [34] for solving nonlinear differential games is of great interest for the theory of differential games and applications.

2. Statement of the Problem

The pursuer P has a fixed speed $w^{(1)}$ but his radius of turn is bounded by a given quantity R. The evader is inertialess. He steers by choosing his velocity vector from the set Q. The kinematic equations are:

$$\begin{aligned} P: \quad & \dot{x}_p = w^{(1)} \sin\psi \\ & \dot{y}_p = w^{(1)} \cos\psi \\ & \dot{\psi} = w^{(1)}\varphi/R, \qquad |\varphi| \le 1 \end{aligned} \qquad\qquad \begin{aligned} E: \quad & \dot{x}_e = v_1 \\ & \dot{y}_e = v_2, \quad v \in Q. \end{aligned}$$

The number of equations can be reduced to two (see [15]) if a coordinate system with the origin at P and the axis x_2 in the direction of P's velocity vector is used (see Figure 1).

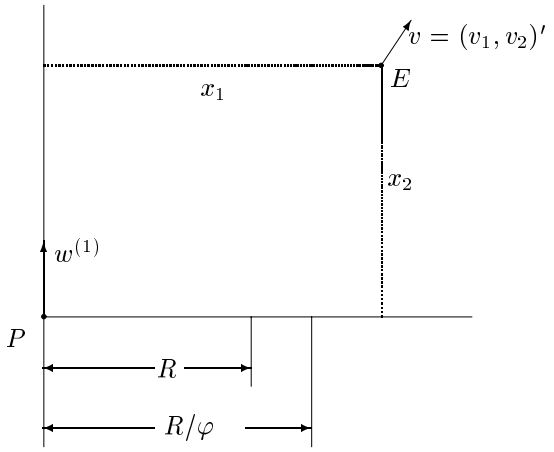

Fig. 1. Homicidal chauffeur dynamics.

The dynamics in the reduced coordinates is

$$\begin{aligned} \dot{x}_1 &= -w^{(1)} x_2\, \varphi/R + v_1 \\ \dot{x}_2 &= \quad w^{(1)} x_1\, \varphi/R + v_2 - w^{(1)}, \qquad |\varphi| \le 1, \quad v \in Q. \end{aligned} \tag{2.1}$$

Here $(x_1,\ x_2)'$ is the state vector which gives the relative position of the evader E with respect to the pursuer P, and $w^{(1)}$ and R are constants which define the pursuer's velocity and the minimal radius of turn, respectively.

2.1. *Homicidal chauffeur game*

The objective of the control φ of the pursuer is to minimize the time of attaining a given terminal set M. The objective of the control $v = (v_1, v_2)'$ of the evader is to maximize this time. Therefore the payoff of the game is the time of attaining the terminal set.

The classical formulation (see [15] and [20]) of the homicidal chauffeur game assumes that the sets M and Q are circles of the radii l (capture radius) and $w^{(2)}$, respectively, with the centers at the origin. It is accepted that $w^{(2)} < w^{(1)}$. With the algorithm proposed, level sets of the value function can be computed for sufficiently wide class of sets M and Q. We assume that Q is a convex compact set and $(0, 0) \in \mathrm{int} Q$.

2.2. *Acoustic game*

The dynamics of the problem is described by (2.1). The difference is that the constraint on the control of player E depends on x. It is given by the formula

$$\mathcal{Q}(x) = k(x)Q, \quad k(x) = \min\{|x|, s\}/s,\ s > 0.$$

Here Q is the same as in section 2.1 and s is a parameter. We have $\mathcal{Q}(x) = Q$ if $|x| \geq s$. The objective of the control φ is to minimize the time of attaining a terminal set M. The objective of the control $v = (v_1, v_2)'$ is to maximize this time.

In this paper, the terminal set M in the form of the rectangle

$$\{(x_1, x_2) \in R^2 : -\alpha \ \leq \ x_1 \ \leq \ \alpha, \ -\beta \leq x_2 \leq 0\}, \quad \alpha > 0, \ \beta > 0$$

will be used. The statement of the acoustic problem with such terminal set was taken from [10]. Very interesting cases from the mathematical point of view arise when the horizontal side of the rectangle is much greater than its vertical side.

2.3. *Conic surveillance-evasion game*

The statement of the problem was given in [19]. The dynamics of the game is described by (2.1). The terminal set M is the complement of the open detection cone depicted in Figure 2. The objective of the control $v = (v_1, v_2)'$ of the evader E is to minimize the time of attaining M. The objective of the control φ of the pursuer P is to maximize this time. Therefore, in contrast to the Isaacs' homicidal chauffeur game, the roles of the players change: the evader is the "minimizing" player and the pursuer is the "maximizing" one.

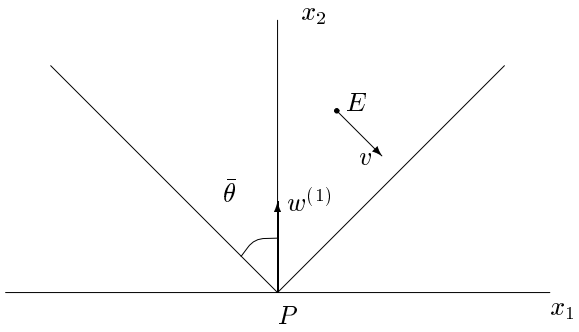

Fig. 2. Detection cone.

In the following, for the uniformity of notation of the constraint of player E, let us agree that $\mathcal{Q}(x) = Q$ for problems 2.1 and 2.3.

2.4. *Level sets of the value function*

We restrict ourself with a conceptual definition of level sets of the value function. The precise definition can be found in [16], [17].

Let $T \geq 0$. The level set (the Lebesgue set) of the value function is denoted by $W(T, M)$. This is the set of all points in the plane such that the minimizing player using feedback strategies can guarantee the transition of trajectories of the system (2.1) to the terminal set M within time T.

3. The Algorithm

In this section, the basic idea of the algorithm for computing sets $W(T,M)$ is described.

The set $W(T,M)$ is formed via a step-by-step backward procedure giving a sequence of embedded sets

$$W(\Delta,M)\subset W(2\Delta,M)\subset W(3\Delta,M)\subset ...\subset W(i\Delta,M)\subset ...\subset W(T,M).$$

Here Δ is the step of the backward procedure. Each set $W(i\Delta,M)$ consists of all initial points from which the minimizing player guarantees the attainment of $W((i-1)\Delta,M)$ within time Δ. We put $W(0,M)=M$.

This is a dynamic programming method. In the theory of differential games, the fundamental ideas of the backward construction of level sets were considered in works of Isaacs, Fleming, Pontryagin, Krasovskii and Pschenichnyi.

The crucial point of our algorithm is the computation of "fronts". The front F_i (Figure 3) is the set of all points of $\partial W(i\Delta,M)$ with the property that the minimal guaranteed time of attaining the previous set $W((i-1)\Delta,M)$ is equal to Δ. For other points of $\partial W(i\Delta,M)$, the optimal time is less than Δ. The line $\partial W(i\Delta,M)\setminus F_i$ possesses the properties of the barrier (see [15] for the definition). The front F_i is computed using the previous front F_{i-1}. For the first step of the backward procedure, F_0 coincides with the usable part (see [15] for the definition) Γ_0 of the boundary of M. It may be one or several usable parts. The computations are carried out separately for each usable part. One should take into account that the obtaining parts of the level set can collide with each other. Below, we will assume for simplicity that only one usable part is on the boundary of M.

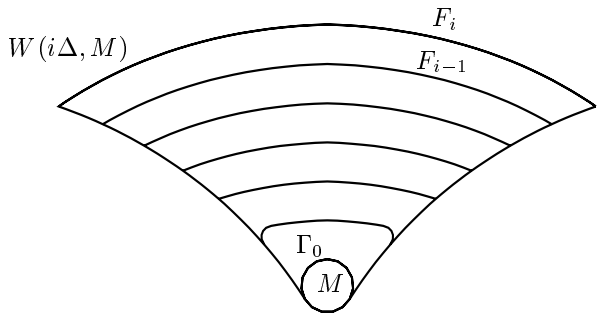

Fig. 3. Construction of the sets $W(i\Delta,M)$.

Let us explain assuming the problems from sections 2.1 and 2.2 how the fronts can be constructed. We write $\mathcal{Q}(x)$ although the constraint $\mathcal{Q}$ of player E does not depend on x in the case of problem 2.1. Using the notation $p(x)=(-x_2,x_1)'\cdot w^{(1)}/R$ and $g=(0,-w^{(1)})'$, we rewrite the equations (2.1) as $\dot{x}=p(x)\varphi+v+g$. First, suppose that the front F_{i-1} is a smooth curve. We distinguish points of local convexity and points of local concavity. In Figure 4, d is a point of local convexity, and e is a point of local concavity. Let x_* be a point of local convexity on F_{i-1}, and

ℓ is the normal vector to the front at x_* directed outside the set $W((i-1)\Delta, M)$. Put $\varphi^\circ = \operatorname{argmin}\{\ell' p(x_*)\varphi : |\varphi| \le 1\}$ and $v^\circ = \operatorname{argmax}\{\ell' v : v \in \mathcal{Q}(x_*)\}$. We call φ° and v° the extremal controls. Similarly, for the points of local convexity, the inner normal vector to the set $W((i-1)\Delta, M)$ at x_* is considered, and the extremal controls $\varphi^\circ = \operatorname{argmax}\{\ell' p(x_*)\varphi : |\varphi| \le 1\}$ and $v^\circ = \operatorname{argmin}\{\ell' v : v \in \mathcal{Q}(x_*)\}$ are introduced. Actually, the distinction of outer and inner normals for cases of local convexity and concavity is convenient when fronts are treated as polygonal lines.

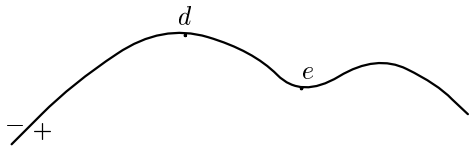

Fig. 4. Local convexity and concavity.

If the vector x_* is collinear to ℓ, then any control $\varphi \in [-1, 1]$ is extremal. If $\mathcal{Q}(x_*)$ is a polygon in the plane, and ℓ is collinear to some normal vector to an edge $[q_1, q_2]$ of $\mathcal{Q}(x_*)$, then any control $q \in [q_1, q_2]$ is extremal.

Using the extremal controls, one computes the extremal trajectories $x(\tau) = x_* - \tau\ (p(x_*)\varphi^\circ + v^\circ + g)$, $\tau \in (0, \Delta]$, started from the front points, in reverse time. The ends of these trajectories at $\tau = \Delta$ are used to form the next front F_i. If the extremal control φ° is not unique at some point $x_* \in F_{i-1}$, then the segment $\Phi(x_*) = \{x_* - \Delta\ (p(x_*)\varphi^\circ + v^\circ + g) :\ \varphi^\circ \in [-1, 1]\}$ is considered instead of the single point. Similarly, if the extremal control v° is not unique, the segment $\Xi(x_*) = \{x_* - \Delta\ (p(x_*)\varphi^\circ + v^\circ + g) :\ v^\circ \in [q_1, q_2]\}$ is considered.

If x_* is a point of local convexity, and the extremal control φ° is not unique, one obtains a local picture like that shown in Figure 5a after computing the extremal trajectories from the point x_*. Here, an additional segment $\Phi(x_*)$ appears on the new front F_i. If the extremal control v° is not unique, a local picture similar to that shown in Figure 5b is obtained. The "swallow tail " $\beta_1\xi\beta_2$ does not belong to the new front F_i, and it is taken away. For points of local concavity, there is an inverse situation: if the extremal control φ° is not unique, a swallow tail that should be removed occurs (Figure 5c); if the extremal control v° is not unique, an additional segment $\Xi(x_*)$ appears on the new front F_i (Figure 5d). If both φ° and v° are non-unique, an insertion or a swallow tail occurs depending on which of segments $\Phi(x_*)$ or $\Xi(x_*)$ is greater.

In the course of numerical computations, we operate with polygonal lines instead of smooth curves. Let the front F_{i-1} is computed. One can divide it into regular parts so that the extremal trajectories emanating from the points of one part do not intersect for $\tau \in (0, \Delta]$. Thus each regular part generates a regular field of extremal trajectories. The ends of these trajectories form an ordered collection of points. Being connected, these points give a polygonal line, which is called the secondary arc. The new front F_i is obtained by processing the regular secondary arcs, the processing being reduced to the intersection of secondary arcs. In Figure 6, the front F_{i-1} consists of two regular parts $[z_1 \cdots z_\omega]$ and $[z_\omega \cdots z_r]$. The ends of

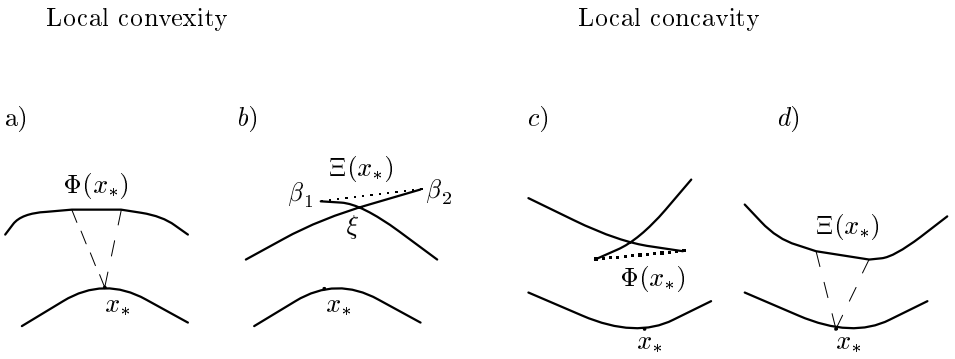

Fig. 5. Nonuniqueness of extremal controls.

the extremal trajectories computed at $\tau = \Delta$ give two secondary arcs, namely $[\xi_1\xi_2\cdots\xi_s]$ and $[\xi_{s+1}\cdots\xi_m]$. The front $F_i = [\xi_1\xi_2\cdots\xi_\alpha\cdots\xi_m]$ is obtained after removing the swallow tail $\xi_s\xi_\alpha\xi_{s+1}$.

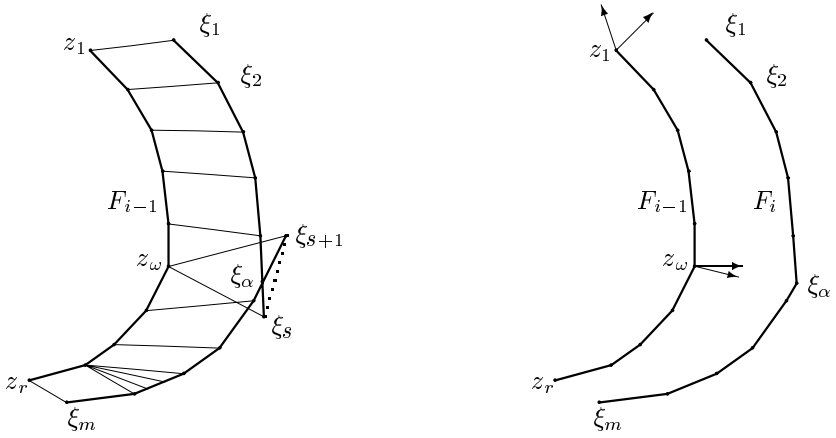

Fig. 6. Computation of fronts.

Unfortunately, very often, it is not sufficient to intersect the neighboring secondary arcs only. In Figure 7, for example, the secondary arcs S_1, S_2 and S_3 are computed sequentially, but the next front is obtained due to the intersection of S_1 and S_3.

The decomposition of the front F_{i-1} into regular parts is being done when processing its vertices. Two normal vectors to the links $[a, b]$ and $[b, c]$ of the polygonal line are considered at each vertex b (Figure 8). At the endpoints of the front, the missing extreme normals are computed from special relations (see [23]). The algorithm treats all possible variants of disposition of the normal vectors $\ell_{[a\,b]}$ and

$\ell_{[bc]}$ to the edges of F_{i-1}, the normals to the edges of $\mathcal{Q}(b)$, and the normals to the segment $\{p(b)\varphi : \ \varphi \in [-1,1]\}$. The vectors b (from the origin to the point b) and $-b$ are used as the normal vectors to the last segment. Figure 8, for instance, shows the case where the vector b is between the vectors $\ell_{[ab]}$ and $\ell_{[bc]}$ and the normals n_1 and n_2 to the set $\mathcal{Q}(b)$ are between the vectors b and $\ell_{[bc]}$. Since b is the point of local convexity, the location of normals to the set $\mathcal{Q}(b)$ between the vectors $\ell_{[ab]}$ and $\ell_{[bc]}$ means that b is one of decomposition points that separate the front F_{i-1} into regular parts. The ends of the extremal trajectories computed at $\tau = \Delta$ give a local picture shown in the left half of Figure 8. Here, four extremal trajectories emerge from the point b. Their ends are $\beta_1, \beta_2, \beta_3$ and β_4. The segment $[\beta_1, \beta_2]$ appears due to nonuniquiness of the extremal control φ° for the vector b. The segments $[\beta_2, \beta_3]$ and $[\beta_3, \beta_4]$ arise due to nonuniquiness of the extremal control v° for the vectors n_1 and n_2. After removing the swallow tail $\beta_2\xi\beta_4$, the polygonal line $\alpha\beta_1\xi\gamma$ becomes a fragment of the next front F_i.

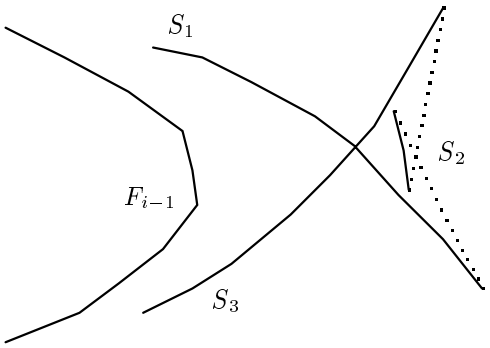

Fig. 7. Secondary arcs: complicated case of disposition.

Some additional details of such local constructions are given in [25]. The main difference from the case of the linear dynamics (see [25]) is that the extremal control of player P can change its value not only at front vertices but also at some interior points of front links. In the game considered, such a switching may occur only once for each front link.

Let us explain the last assertion. Let K be a straight line and ℓ its normal vector. Since the restriction of the scalar function $\ell' p(x)$ to K is a linear function in x, the expression $\ell' p(x)$ can change its sign only once for $x \in K$. Therefore, the extremal control of player P, which is determined by the formula $\operatorname{argmin}\{\ell' p(x)\varphi : |\varphi| \le 1\}$, can switch only once if x runs through K. The switching happens at the point $\bar{x} \in K$ for which the vector $\bar{x}$ is orthogonal to K. If $0 \in K$, then $\bar{x} = 0$.

In order to take into account the dependence of the constraint of player E on x, other additional division points on the front links may also be introduced.

In the case of surveillance-evasion game from section 2.3, the players change their roles: the extremal controls of the pursuer P and the evader E are determined via the relations $\varphi^\circ = \operatorname{argmax}\{\ell' p(x_*)\varphi : |\varphi| \le 1\}$ and $v^\circ = \operatorname{argmin}\{\ell' v : v \in Q\}$,

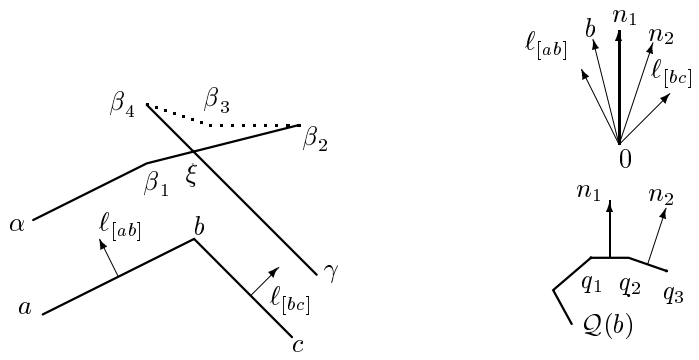

Fig. 8. Example of local constructions.

for every point x_* of local convexity and outer normal ℓ to the front at x_*. For the points of local concavity, the extremal controls of P and E are defined by the formulae $\varphi^\circ = \operatorname{argmin}\{\ell' p(x_*)\varphi : |\varphi| \le 1\}$ and $v^\circ = \operatorname{argmax}\{\ell' v : v \in Q\}$, where ℓ is an inner normal to the front at x_*. So, the local constructions described earlier for the points of local convexity are now true for the points of local concavity and vice versa.

4. Semipermeable Curves in Differential Games with the Homicidal Chauffeur Dynamics

In this section, the results of some analysis of families of smooth semipermeable curves in differential games with homicidal chauffeur dynamics will be given. The semipermeable curves can be helpful for checking the computation of level sets of the value function.

The families of semipermeable curves are determined from only the dynamics of the system and the bounds on the controls of the players.

We explain now what semipermeable curves mean (see also [15]). Let

$$H(\ell, x) = \min_{|\varphi|\le 1} \max_{v\in\mathcal{Q}(x)} \ell' f(x,\varphi,v) = \max_{v\in\mathcal{Q}(x)} \min_{|\varphi|\le 1} \ell' f(x,\varphi,v), \quad x \in R^2,\ \ell \in R^2 \quad (4.2)$$

be the Hamiltonian of the game. Here $f(x,\varphi,v) = p(x)\varphi + v + g$. Fix $x \in R^2$ and consider ℓ such that $H(\ell, x) = 0$. Letting $\varphi^* = \operatorname{argmin}\{\ell' p(x)\varphi\colon\ |\varphi| \le 1\}$ and $v^* = \operatorname{argmax}\{\ell' v\colon\ v \in \mathcal{Q}(x)\}$, it follows that $\ell' f(x,\varphi^*,v) \le 0$ holds for any $v \in \mathcal{Q}(x)$, and $\ell' f(x,\varphi,v^*) \ge 0$ holds for any $\varphi \in [-1,1]$. This means that the direction $f(x,\varphi^*,v^*)$, which is orthogonal to ℓ, separates the vectograms $U(v^*) = \{f(x,\varphi,v^*)\colon\ \varphi \in [-1,1]\}$ and $V(\varphi^*) = \{f(x,\varphi^*,v)\colon\ v \in \mathcal{Q}(x)\}$ of players P and E as in Figure 9. Such a direction is called semipermeable. A smooth curve is called a semipermeable curve if the tangent vector at any point of this curve is a semipermeable direction.

The number of semipermeable directions depends on the form of the function $\ell \to H(\ell, x)$ at the point x. In the case considered, the function $H(\cdot, x)$ is composed

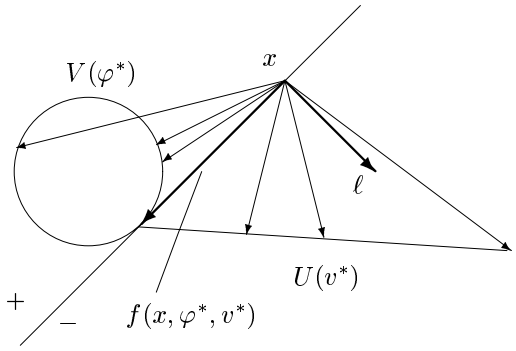

Fig. 9. Semipermeable direction.

of two convex functions:

$$H(\ell,x)=\begin{cases}\max\limits_{v\in\mathcal{Q}(x)}\ell'v+\ell'p(x)+\ell'g, & \text{if } \ell'p(x)<0\\ \max\limits_{v\in\mathcal{Q}(x)}\ell'v-\ell'p(x)+\ell'g, & \text{if } \ell'p(x)\geq 0.\end{cases}$$

The semipermeable directions are derived from the roots of the equation $H(\ell,x)=0$. We will distinguish the roots "$-$" to "$+$" and the roots "$+$" to "$-$". When classifying these roots, we suppose that $\ell\in\mathcal{E}$, where $\mathcal{E}$ is the boundary of a convex polygon containing the origin. We say that ℓ_* is a root $-$ to $+$ if $H(\ell_*,x)=0$, and if $H(\ell,x)<0$ ($H(\ell,x)>0$) for $\ell<\ell_*$ ($\ell>\ell_*$) that are sufficiently close to ℓ_*, where the notation $\ell<\ell_*$ means that the direction of the vector ℓ can be obtained from the direction of the vector ℓ_* using a counterclockwise rotation through an angle not exceeding π. The roots $-$ to $+$ and the roots $+$ to $-$ are called roots of the first and second type, respectively.

We denote roots of the first type by $\ell^{(1),i}(x)$ and roots of the second type by $\ell^{(2),i}(x)$. The right index takes the value 1 or 2, and indicates the half-plane $\{\ell\in R^2:\ \ell'p(x)<0\}$ or $\{\ell\in R^2:\ \ell'p(x)\geq 0\}$. Figure 10 explains the appearance of four roots in terms of vectograms. The upper and lower circles are the vectograms of player E for $\varphi=1$ and $\varphi=-1$, respectively.

Due to the above mentioned property of the piecewise convexity of the function $H(\cdot,x)$, the equation $H(\ell,x)=0$ can have at most two roots of each type for any given x.

We now describe how the families of smooth semipermeable curves can be constructed.

4.1. *Constraint $\mathcal{Q}$ on the control of player E does not depend on x*

Assume that the constraint $\mathcal{Q}$ does not depend on x that is $\mathcal{Q}(x)=Q$. Denote

$$A_*=\{(x_1,x_2):\ x_1=\frac{v_2R}{w^{(1)}}-R,\ \ x_2=-\frac{v_1R}{w^{(1)}},\ (v_1,v_2)'\in Q\},\tag{4.3}$$

$$B_*=\{(x_1,x_2):\ x_1=-\frac{v_2R}{w^{(1)}}+R,\ \ x_2=\frac{v_1R}{w^{(1)}},\ (v_1,v_2)'\in Q\}.\tag{4.4}$$

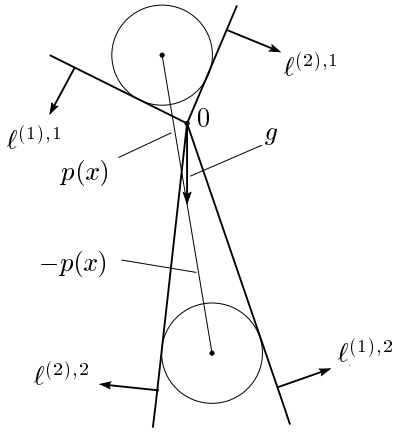

Fig. 10. Appearance of four roots.

The set B_* is symmetric to the set A_* with respect to the origin. Let $C_* = A_* \bigcap B_*$.

1. Let us show for all $x \notin C_*$ that the equation $H(\ell, x) = 0$ has at least one root of the first type and one root of the second type. To prove this, it is sufficient to verify that, for any x, there exist vectors $\underline{\ell}$ and $\overline{\ell}$ such that $H(\underline{\ell}, x) < 0$ and $H(\overline{\ell}, x) > 0$.

Let $x \notin A_*$. Then there exists a vector $\widetilde{\ell}$ such that $\widetilde{\ell}'x > \widetilde{\ell}'z$ for any $z \in A_*$. That is

$$-\widetilde{\ell}'x + \max_{z \in A_*} \widetilde{\ell}'z < 0.$$

Denote by $\overline{x}$ the nearest to x point of A_*. The vector $x - \overline{x}$ can be considered as $\widetilde{\ell}$.

Assume $\underline{\ell} = \left(-\widetilde{\ell}_2 R/w^{(1)},\ \widetilde{\ell}_1 R/w^{(1)}\right)'$. We have

$$H(\underline{\ell},\ x) \le \underline{\ell}' \left(\frac{w^{(1)}x_2}{R},\ \frac{-w^{(1)}x_1}{R}\right)' + \underline{\ell}'g + \max_{v \in Q} \underline{\ell}'v = -\widetilde{\ell}_2 x_2 - \widetilde{\ell}_1 x_1 - \widetilde{\ell}_1 R +$$

$$\max_{v \in Q} \left(\frac{-\widetilde{\ell}_2 R}{w^{(1)}} v_1 + \frac{\widetilde{\ell}_1 R}{w^{(1)}} v_2\right) = -\widetilde{\ell}'x + \max_{v \in Q} \widetilde{\ell}' \left(\frac{v_2 R}{w^{(1)}} - R,\ \frac{-v_1 R}{w^{(1)}}\right)' =$$

$$-\widetilde{\ell}'x + \max_{z \in A_*} \widetilde{\ell}'z < 0.$$

Similarly, one can show for $x \notin B_*$ that there exists a vector $\underline{\ell}$ such that $H(\underline{\ell},\ x) < 0$. Therefore, if $x \notin C_*$, then there exists a vector $\underline{\ell}$ such that $H(\underline{\ell},\ x) < 0$.

Consider $\overline{\ell} \neq 0$ such that $\overline{\ell}'p(x) = 0$ and $\overline{\ell}'g \ge 0$. With the assumption $0 \in \mathrm{int}Q$, one derives

$$H(\overline{\ell}, x) = \max_{v \in Q} \overline{\ell}'v + \overline{\ell}'g > 0.$$

This completes the proof.

Let $x \in \mathrm{int}C_*$. We show that $H(\ell,\ x) > 0$ for all $\ell \neq 0$. Take $\ell \neq 0$. Suppose that $\min\{\ell' p(x)\varphi : \varphi \in [-1,1]\}$ occurs for $\varphi = -1$ ($\varphi = 1$). It follows from the definition of the set A_* (B_*) that for $x \in \mathrm{int}A_*$ ($x \in \mathrm{int}B_*$), there exists a vector $v_* \in \mathrm{int}Q$ such that $f(x,\ -1,\ v_*) = 0$ ($f(x,\ 1,\ v_*) = 0$). Hence, $H(\ell,\ x) > 0$. Therefore, roots of the first and second type do not exist for $x \in \mathrm{int}C_*$. Due to continuity of H, strict roots do not exist for $x \in \partial C_*$ too.

2. Suppose $C_* = \emptyset$. Consider cones spanned onto the sets A_* and B_* with the apex at the origin. Denote these cones by coneA_* and coneB_*, respectively. The part of coneA_* after deleting the set

$$\{(x_1, x_2) :\ x_1 = \frac{v_2 R}{w^{(1)}\varphi} - R/\varphi,\ x_2 = -\frac{v_1 R}{w^{(1)}\varphi},\ 1 < \varphi < \infty,\ (v_1, v_2)' \in Q\}$$

is denoted by A. Similarly, the set B as the part of coneB_* is introduced.

One can find the domains of the functions $\ell^{(j),i}(\cdot)$, $j = 1,2$, $i = 1,2$. The domains are identical for problems 2.1 and 2.3 if the set Q is the same.

Figure 11 presents the sets A and B and the domains of the functions $\ell^{(j),i}(\cdot)$, $j = 1,2$, $i = 1,2$, for the case where the set Q is a polygonal approximation of a circle of some radius $w^{(2)}$ with the center at the origin. The boundaries of A and B are drawn with the thick lines. There exist two roots of the first type and two roots of the second type at each internal point of the sets A and B. For any point in the exterior of A and B, there exist one root of the first type and one root of the second type.

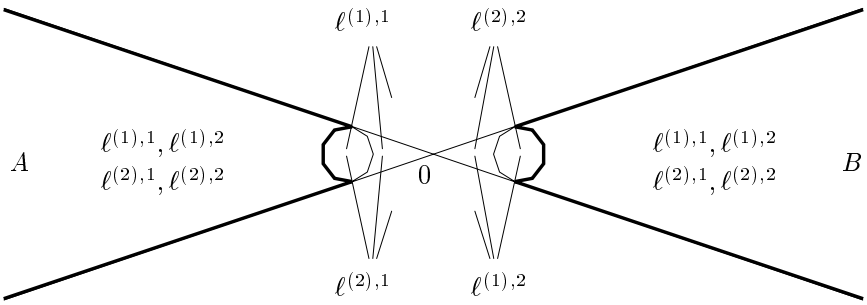

Fig. 11. Domains of $\ell^{(j),i}$. Set $\mathcal{Q}$ does not depend on x; $C_* = \emptyset$.

The sets analogous to that shown in Figure 11 were used in [15] and [18]–[20] to construct semipermeable curves. Here, the modification consists in that the roots of the first and second types are being distinguished and the corresponding semipermeable curves of the first and second types are considered.

The function $\ell^{(j),i}(\cdot)$ is Lipschitz continuous on any closed bounded subset of the interior of its domain. One can consider the two-dimensional differential equation

$$dx/dt = \Pi\ell^{(j),i}(x), \tag{4.5}$$

where Π is the matrix of rotation through the angle $\pi/2$, the rotation being clockwise or counterclockwise if $j = 1$ or $j = 2$, respectively. Since the tangent vector at each point of the trajectory defined by this equation is a semipermeable direction, the trajectories are semipermeable curves. Therefore player P can keep the state vector x on one side of the curve (positive side), and player E can keep x on the other (negative) side. Further, equation (4.5) specifies a family $\Lambda^{(j),i}$ of smooth semipermeable curves.

The families $\Lambda^{(j),i}$, $j = 1, 2$, $i = 1, 2$, for the games from sections 2.1 and 2.3 in the case $C_* = \emptyset$ are depicted in Figure 12. Each smooth semipermeable curve is a trajectory of system (2.1) for controls of the players that deliver minimum and maximum in (4.2). The arrows show the direction of motion in reverse time. Note that all the pictures can be obtained from one picture by reflections in the x_1- and x_2-axes.

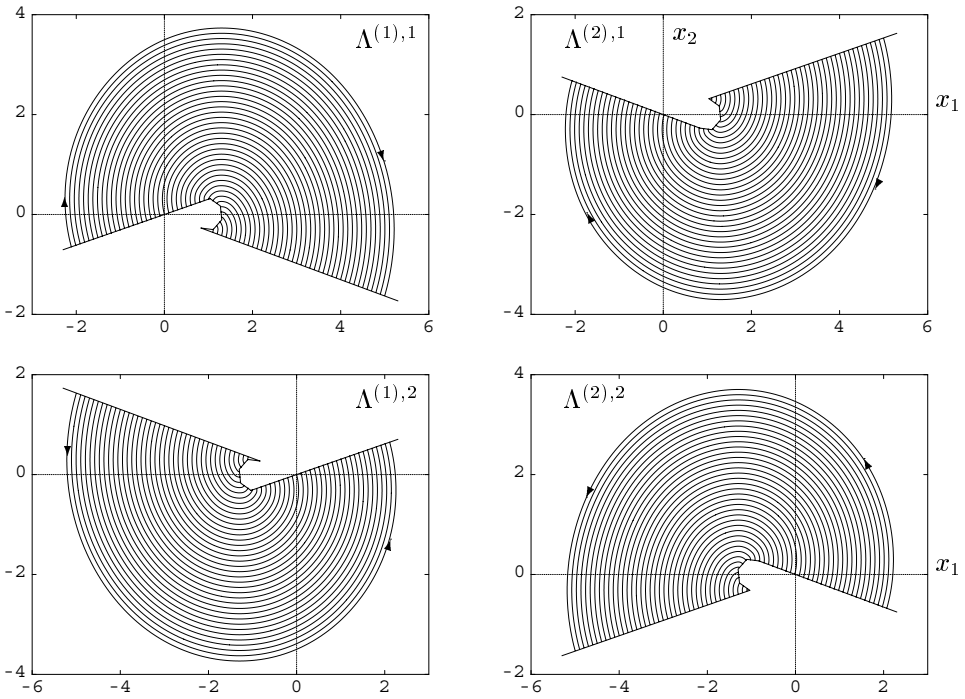

Fig. 12. Families of semipermeable curves. Set $\mathcal{Q}$ does not depend on x; $C_* = \emptyset$.

3. Let now $C_* \neq \emptyset$. There are no roots in the set C_*, there are four roots in the set $R^2 \setminus (A_* \bigcup B_*)$, and there are two roots (one root of the first type and one root of the second type) in the rest part of the plane that is in $(A_* \bigcup B_*) \setminus C_*$. Figure 13 shows the domains of the functions $\ell^{(j),i}(\cdot)$ for this case. The set Q is a circle of some radius $w^{(2)} > w^{(1)}$ with the center at the origin. The digits 4, 2 and 0 state the number of roots.

Using (4.5), one can produce the families $\Lambda^{(j),i}$ for the case where $C_* \neq \emptyset$.

Figure 14 presents the family $\Lambda^{(1),1}$. The initial points for emitting the semipermeable curves are uniformly distributed over the circumference of radius 4 with the center at the origin. The families $\Lambda^{(1),2}$, $\Lambda^{(2),1}$ and $\Lambda^{(2),2}$ can be obtained from $\Lambda^{(1),1}$ by reflections in the x_1- and x_2-axes.

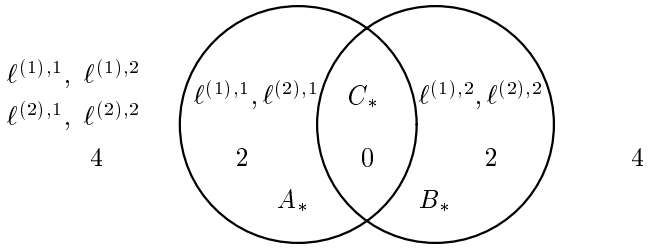

Fig. 13. Domains of $\ell^{(j),i}(\cdot)$. Set $\mathcal{Q}$ does not depend on x; $C_* \neq \emptyset$.

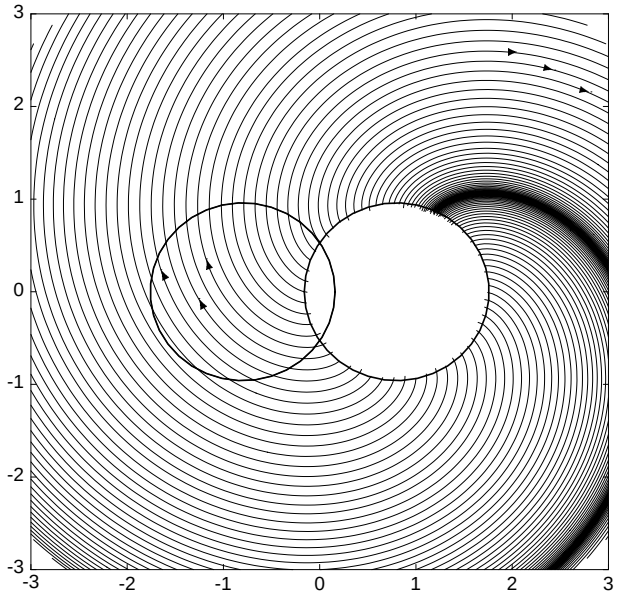

Fig. 14. Family of semipermeable curves for the root $\ell^{(1),1}$. Set $\mathcal{Q}$ does not depend on x; $C_* \neq \emptyset$.

The curves of families belonging to the same type can be sewed so that the semipermeability property will be preserved for obtaining composite (see [6], [8] and [21]) curve. Such a sewing for semipermeable curves of the first (second) type is only possible if the sewing point belongs to certain parts of the boundaries of the sets where the families $\Lambda^{(1),1}$ and $\Lambda^{(1),2}$ ($\Lambda^{(2),1}$ and $\Lambda^{(2),2}$) are defined. The composite curve of the first or second type can be smooth in some cases. Very often,

the boundary of the solvability set is formed by composite curves (see, for example, [19], [21]–[23] and [32]).

The following important property holds true for any point $x \in C_* = A_* \bigcap B_*$:

$$\text{for any } \varphi \in [-1,1] \text{ there exists } v \in Q \text{ such that } f(x,\varphi,v) = 0.$$

Therefore, in the region C_*, player E can counter any control of player P, so the state remains immovable all the time. Further, if a point x with the above property does not belong to the terminal set M, then M can not be reached from x. We call regions of such points the superiority sets of player E.

4.2. *Constraint $\mathcal{Q}$ on the control of player E depends on x*

Using the form of the domains of $\ell^{(j),i}(\cdot)$ from section 4.1, one can construct the domains for problem 2.2 with $\mathcal{Q}(x) = k(x)Q$, where $k(x) = \min\{|x|,\ s\}/s,\ s > 0$.

Let us describe schematically how it can be done. We have $\mathcal{Q}(x) = Q$ outside the circle of radius s with the center at the origin. Inside the circle of radius s, the coefficient $k(x)$ is proportional to $|x|$.

First note that $k(x) = \text{const}$ for the points x of any circumference of some fixed radius with the center at $(0,0)$. It holds $k(x) = 1$ outside the circle of radius s. Take a circumference $\Omega(r)$ of radius r with the center at $(0,0)$. Set $k(r) = \min\{r,\ s\}/s$ and $Q(r) = k(r)Q$. We have $\mathcal{Q}(x) = Q(|x|)$.

Form the sets $A_*(r)$ and $B_*(r)$ substituting the set $Q(r)$ instead of Q in formulae (4.3) and (4.4) for A_* and B_*. Let $C_*(r) = A_*(r) \bigcap B_*(r)$. Using $A_*(r)$ and $B_*(r)$, construct domains of $\ell^{(j),i}(\cdot)$, the cases $C_*(r) = \emptyset$ and $C_*(r) \neq \emptyset$ being distinguished. Put the circumference $\Omega(r)$ onto the constructed domains. As a result, a division of the circumference onto arcs is obtained. The number and the type of roots are the same for all points of each arc. This technique is applied for every r in $[0,s]$, and identically named division points are connected. Thus the circle of radius s is divided into parts according to the kinds of roots. Outside this circle, the dividing lines coincide with the lines constructed for the case when $\mathcal{Q}$ does not depend on x.

We now explain the described procedure for the case when Q is a circle of radius w_e with the center at the origin. In this case, $Q(r)$ is the circle of radius $w^{(2)}(r) = \min\{r,\ s\}w_e/s$. The condition $C_*(r) = \emptyset$ means that $w^{(2)}(r) < w^{(1)}$, and the condition $C_*(r) \neq \emptyset$ is equivalent to the relation $w^{(2)}(r) \geq w^{(1)}$. If $w^{(2)}(r) \leq w^{(1)}$, we put the points $x \in \Omega(r)$ onto the domains of Figure 11 constructed for $w^{(2)} = w^{(2)}(r)$. Otherwise, if $w^{(2)}(r) > w^{(1)}$, we put these points onto the domains of Figure 13. In Figure 15a, the division points a, b, c and d, and those symmetric to them in the left half-plane, are shown, $\Omega(r)$ being the dotted line. In Figure 15b, the division points e and f, and those symmetric to them, are depicted.

Figures 16, 18 and 20 were constructed in this way for the parameters $w^{(1)} = 1$, $R = 0.8$, $s = 0.75$ and $w_e = 0.8,\ 1.8$ and 2. In Figure 16, the domains of the functions $\ell^{(j),i}(\cdot)$ are shown, and also the sets that are analogous to A and B in Figure 11 are marked. In Figure 18, two symmetric superiority sets of player E arise, the upper set being denoted by C_U and the lower set by C_L. If we increase w_e, the sets C_U and C_L expand and form a doubly connected region that is denoted by C_* in Figure 20. The number of roots of the equation $H(\ell, x) = 0$ is also given

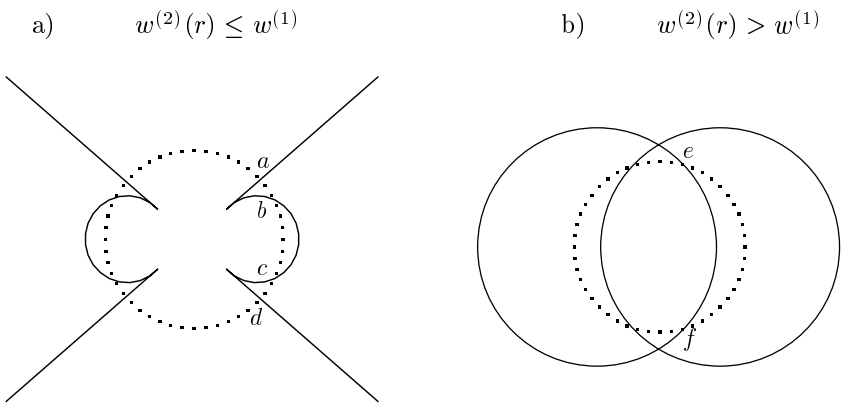

Fig. 15. Construction of domains of functions $\ell^{(j),i}(\cdot)$.

in Figures 16, 18 and 20. Arcs which separate the domains of the functions $\ell^{(j),i}$ (and are similar to that in the central part of Figure 16) are not included. In Figures 17, 19 and 21, the family $\Lambda^{(1),1}$ of semipermeable curves for the values of parameters corresponding to Figures 16, 18 and 20 is shown.

5. Formation of Holes in Solvability Sets due to Superiority Sets

The role of superiority sets in the appearance of holes within the solvability sets will be explained in this section. For the surveillance-evasion game, the existence of superiority sets of player E can not be a cause for the arising of holes because the objective of E is to bring the state to the terminal set M. Therefore the considerations of this section are related to problems 2.1 and 2.2.

We will suppose here that the set Q is a circle of radius w_e with the center at the origin.

As noted above, in the case of problem 2.2, there can be one doubly connected superiority set C_* of player E, or two simply connected sets C_U and C_L, or the superiority set can be empty. In the case of problem 2.1, the superiority set of player E can be simply connected or empty.

1. Let D be a closed set. Assume that the objective of player E is to bring the state of the system to the set D. Denote by $\hat{D}$ the maximal solvability set (victory domain) of player E. It follows from the definition of $\hat{D}$ that E can bring the state of the system to D from any point $x \in \hat{D}$, but player P can prevent the state of the system from approaching the set D for any point $x \notin \hat{D}$. The boundary of $\hat{D}$ is composed of smooth semipermeable curves of the families $\Lambda^{(j),i}$. The sewing points possess the semipermeability property (see [11]). In some cases, a part of the boundary of $\hat{D}$ can coincide with a part of the boundary of D.

Below, the set C_* or one of the sets C_U and C_L is used as the set D. Since in this case, D is a superiority set of E, it possesses the property of v-stability (see [16] and [17] for the definition) or, in other terms, the property of viability for E (see [1] and [10]), and the set $\hat{D}$ is v-stable too. This means that player E can hold the trajectories of the system in $\hat{D}$ for infinite time. Hence, if $\hat{D} \bigcap M = \emptyset$, then the

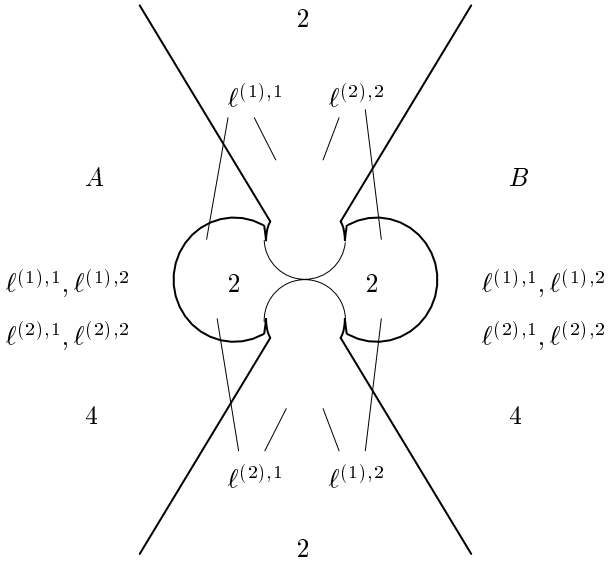

Fig. 16. Domains of $\ell^{(j),i}(\cdot)$. Set $\mathcal{Q}$ depends on x; $w_e = 0.8$.

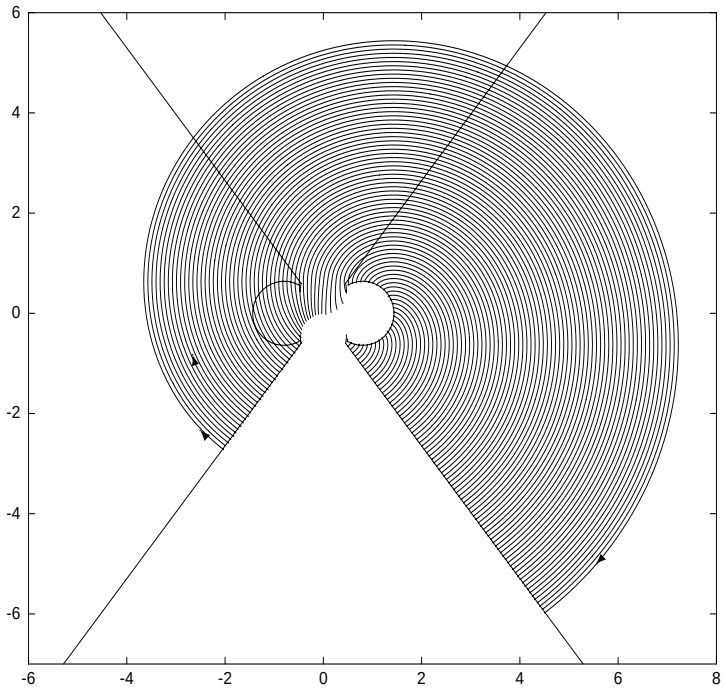

Fig. 17. Family of semipermeable curves for the root $\ell^{(1),1}$. Set $\mathcal{Q}$ depends on x; $w_e = 0.8$.

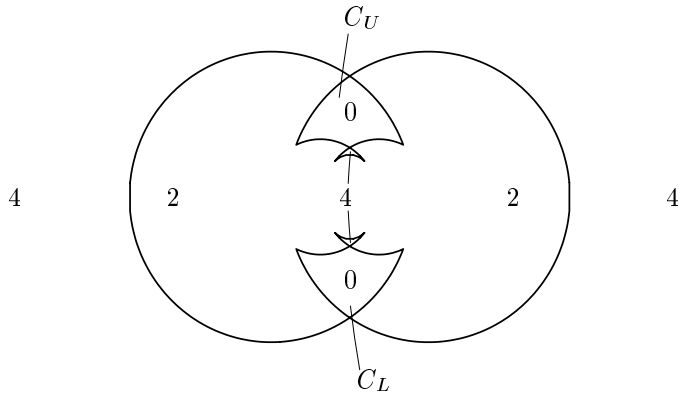

Fig. 18. Superiority sets C_U and C_L of player E. Set $\mathcal{Q}$ depends on x; $w_e = 1.8$.

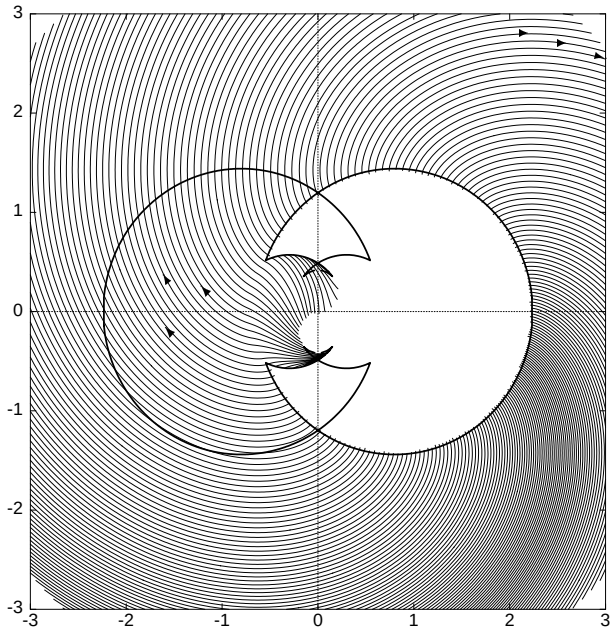

Fig. 19. Family of semipermeable curves for the root $\ell^{(1),1}$. Set $\mathcal{Q}$ depends on x; $w_e = 1.8$.

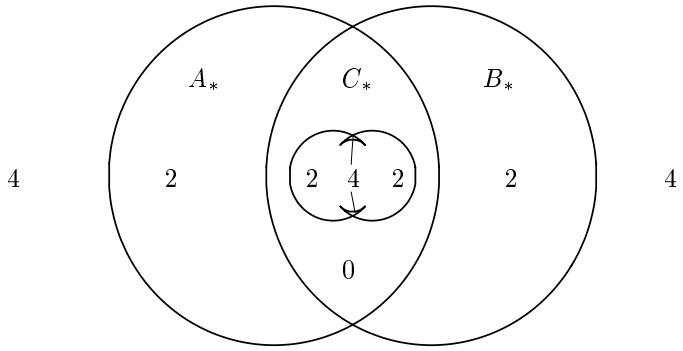

Fig. 20. Superiority set C_* of player E. Set $\mathcal{Q}$ depends on x; $w_e = 2$.

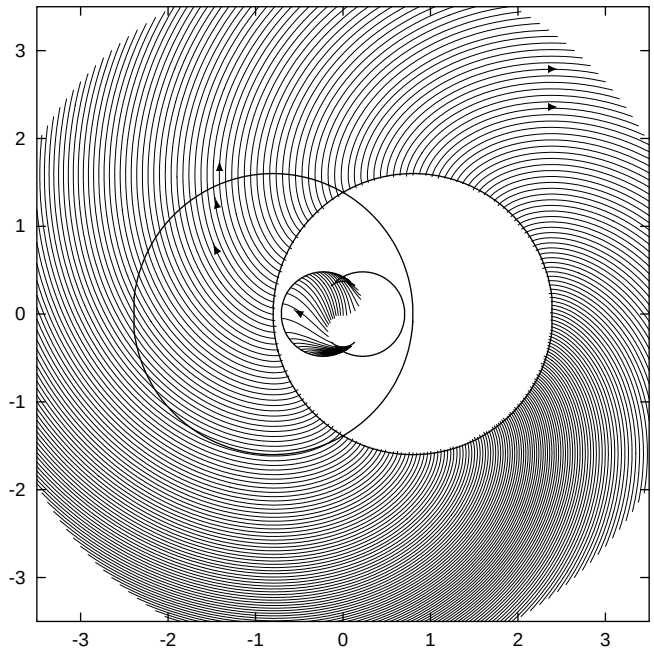

Fig. 21. Family of semipermeable curves for the root $\ell^{(1),1}$. Set $\mathcal{Q}$ depends on x; $w_e = 2$.

time for achieving the terminal set M in the main problem is infinite for any point x in $\hat{D}$. For this reason, level lines of the value function can not "penetrate" into the set $\hat{D}$.

Due to the simple geometry of the sets D of the problem considered, the sets $\hat{D}$ can be obtained easily using the families of semipermeable curves. For example, Figure 22a presents the configuration of $\hat{C}_U$. The values of parameters correspond to Figures 18 and 19. The sewing point of the curves $p^{(2),2}$ and $p^{(1),2}$, and symmetric to it sewing point of the curves $p^{(1),1}$ and $p^{(2),1}$, lie on the boundary of C_U. In Figure 22b, an example of the set $\hat{C}_L$ is given. The same values of parameters as for Figure 22a are used.

Figure 23a shows the set $\hat{D} = \hat{C}_*$ for the case when the sets C_U and C_L are merged in the set C_*. A similar structure of the set $\hat{D}$ is obtained if $\mathcal{Q}$ does not depend on x (see Figure 23b).

Since level lines of the value function can not penetrate into the set $\hat{D}$ in the case $\hat{D} \bigcap M = \emptyset$, one can try to generate examples with holes in solvability sets using the knowledge of the geometry of the sets $\hat{D}$. The construction of such examples is only possible on the base of a set C_U. We will show that only sets $\hat{C}_U$, but not sets $\hat{C}_L$ or $\hat{C}_*$ can occur as the holes.

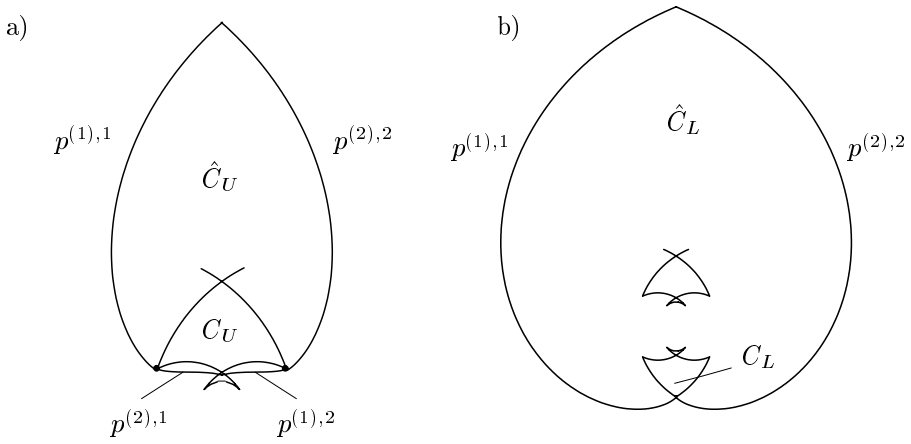

Fig. 22. Construction of the sets $\hat{C}_U$ and $\hat{C}_L$ on the base of the superiority sets C_U and C_L.

2. Let us explain why a set $\hat{C}_L$ can not occur as the hole. For the set C_L, a collection of expanding v-stable sets can be easily obtained. Figure 24a shows such a collection computed for the set C_L from Figures 18, 19 and 22b. The first set of the collection is $\hat{C}_L$. The boundaries of the sets are formed by the semipermeable curves $p^{(1),1}$ and $p^{(2),2}$ which are symmetric with respect to the axis x_2.

Figure 24b shows the semipermeable curves that form the boundary of some set S from the above collection. The curve $p^{(1),1}$ corresponds to the control $\varphi = 1$, but the curve $p^{(2),2}$ corresponds to the control $\varphi = -1$. The sign "+" ("−") marks those sides of semipermeable curves that player P (E) keeps. The curves $p^{(1),1}$ and $p^{(2),2}$

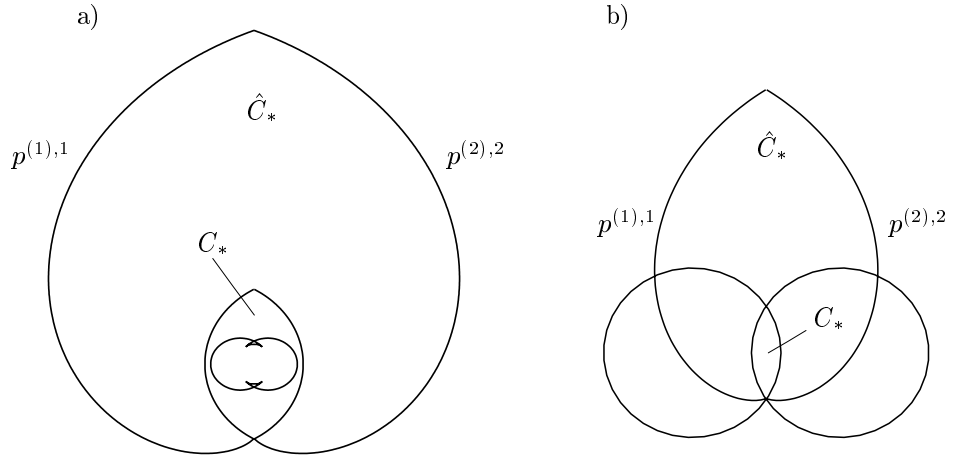

Fig. 23. Structure of sets $\hat{C}_*$. a: $\mathcal{Q}$ depends on x; b: $\mathcal{Q}$ does not depend on x.

are faced with negative sides at the intersection point a. The property of v-stability means the following: for any $x \in \partial S$ and any $\varphi \in [-1,\ 1]$ there exists $v \in \mathcal{Q}(x)$ such that the vector $f(x,\ \varphi,\ v)$ is directed inside the set S or it is tangent to the boundary of S at x. For any point $x \in \partial S$ excluding the point a, every $v \in \mathcal{Q}(x)$ that gives the maximum in (4.2) would be appropriate. A normal vector to the semipermeable curve in the negative side direction is considered as ℓ when

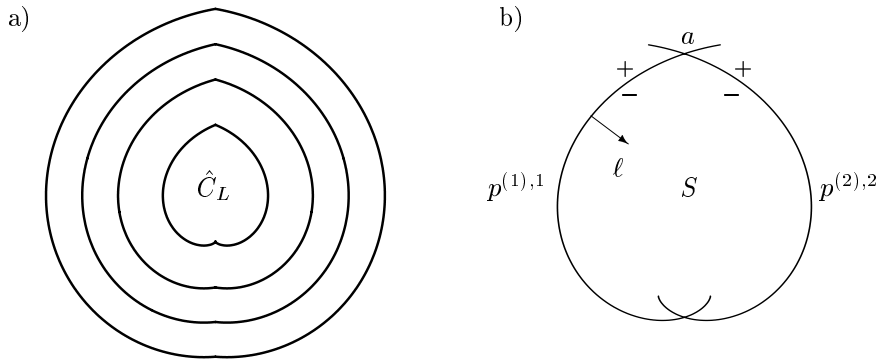

Fig. 24. a: Collection of expanding v-stable sets for the set C_L. b: Explanation of v-stability.

computing the maximum in (4.2). For the point a, the choice of an appropriate v depends on φ.

Let us assume that there exists a hole $\hat{C}_L$ which is located strictly inside the solvability set. It follows from this assumption that: 1) $\hat{C}_L \bigcap M = \emptyset$, 2) for any boundary point x of $\hat{C}_L$, there exist points of the fronts that are arbitrarily close to x.

Consider a v-stable set $\bar{S}$ from the expanding collection generated by the set C_L and such that $\bar{S}$ and M have common points on the boundaries of $\bar{S}$ and M only. Take a point x on a front strictly inside the set $\bar{S}$. Such a point exists because the set $\hat{C}_L$ belongs to the interior of the set $\bar{S}$ and the fronts come arbitrarily close to the set $\hat{C}_L$. Then, player E can keep the trajectories of the system within a set $\widetilde{S}$, which is a subset of $\bar{S}$ and contains the point x on its boundary, for infinite time. This contradicts to the fact that x lies on the front and, therefore, player P brings the system to M for a finite time.

Similar arguments are true for sets $\hat{C}_*$ arising in the acoustic or classical game.

3. Let us now consider the situation with the set $\hat{C}_U$.

Denote by $r^\flat = w^{(1)}s/w_e$ the minimal r for which $C_*(r) \neq \emptyset$. Consider the circle $F(\widetilde{r})$ of radius $\widetilde{r} = r^\flat/2$ with the center at the origin. We have

$$w^{(1)} - w^{(2)}(|x|) \geq w^{(1)} - w^{(2)}(\widetilde{r}) = \frac{w^{(1)}}{2}, \quad x \in F(\widetilde{r}). \tag{5.6}$$

Let

$$\xi(r) = -R + \frac{w^{(2)}(r)R}{w^{(1)}}, \quad r \geq 0. \tag{5.7}$$

Since the set C_U is strictly above the axis x_1, then, for any $r \geq 0$, the set $C_*(r)$ does not contain the points of intersection of the circumference $\Omega(r)$ of radius r and the center at the origin with the axis x_1. Hence

$$r > \xi(r). \tag{5.8}$$

Let $x^\#(r,\ \alpha)$ and $x^\diamondsuit(r,\ \alpha)$ are right and left intersection points of the straight line $x_2 = \alpha$ with the circumference $\Omega(r)$, $\ 0 \leq \alpha \leq \widetilde{r}$, $\ r \geq \widetilde{r}$. Using (5.7) and (5.8), choose $\widetilde{\beta}$ and $\widetilde{\alpha}$, $\widetilde{\alpha} \leq \widetilde{r}$, so that

$$x_1^\#(r,\ \alpha) \geq \widetilde{\beta} + \xi(r), \quad r \geq \widetilde{r}, \quad 0 \leq \alpha \leq \widetilde{\alpha}. \tag{5.9}$$

We obtain simultaneously

$$x_1^\diamondsuit(r,\ \alpha) \leq -\widetilde{\beta} - \xi(r), \quad r \geq \widetilde{r}, \quad 0 \leq \alpha \leq \widetilde{\alpha}. \tag{5.10}$$

Denote by $X(\alpha) = \{x:\ 0 < x_2 \leq \alpha\},\ \alpha \leq \widetilde{\alpha}$, a horizontal strip of the width α over the axis x_1.

Using (5.9), we obtain $x_1 \geq \widetilde{\beta} + \xi(|x|)$ for the points $x \in X(\widetilde{\alpha})$ on the right of the circle $F(\widetilde{r})$. Hence, it holds

$$\dot{x}_2|_{\varphi=-1} = -x_1\frac{w^{(1)}}{R} + v_2 - w^{(1)} \leq -\widetilde{\beta}\frac{w^{(1)}}{R} - w^{(2)}(|x|) +$$

$$w^{(1)} + v_2 - w^{(1)} \leq -\widetilde{\beta}\frac{w^{(1)}}{R} \tag{5.11}$$

for any $v \in \mathcal{Q}(x)$ and $\varphi = -1$.

Similarly, using (5.10), we get

$$\dot{x}_2|_{\varphi=1} = x_1\frac{w^{(1)}}{R} + v_2 - w^{(1)} \le -\widetilde{\beta}\frac{w^{(1)}}{R} \tag{5.12}$$

for $x \in X(\widetilde{\alpha})$ on the left of the circle $F(\widetilde{r})$, any $v \in \mathcal{Q}(x)$ and $\varphi = 1$.

If a point $x \in X(\widetilde{\alpha})$ that belongs to the circle $F(\widetilde{r})$ satisfies the inequality $x_1 \ge \xi(\widetilde{r})/2 = -R/4$, then we obtain

$$\dot{x}_2|_{\varphi=-1} = -x_1\frac{w^{(1)}}{R} + v_2 - w^{(1)} \le \frac{1}{4}w^{(1)} + v_2 - w^{(1)} \le -\frac{1}{4}w^{(1)} \tag{5.13}$$

for any $v \in \mathcal{Q}(x)$ and $\varphi = -1$. It was taken into account here that, using (5.6), the relation $|v_2| \le w^{(2)}(|x|) \le w^{(2)}(\widetilde{r}) = w^{(1)}/2$ holds for $x \in F(\widetilde{r})$.

Similarly, if a point $x \in X(\widetilde{\alpha})$ belongs to the circle $F(\widetilde{r})$ and satisfies the inequality $x_1 \le R/4$, then we get

$$\dot{x}_2|_{\varphi=1} = x_1\frac{w^{(1)}}{R} + v_2 - w^{(1)} \le -\frac{1}{4}w^{(1)} \tag{5.14}$$

for any $v \in \mathcal{Q}(x)$ and $\varphi = 1$.

Denote

$$\widetilde{\gamma} = \min\{\widetilde{\beta}\frac{w^{(1)}}{R},\ \frac{1}{4}w^{(1)}\}.$$

Take positive $\overline{\alpha} \le \min\{\widetilde{\alpha},\ \widetilde{r}/2\}$ such that

$$\frac{\overline{\alpha}}{\widetilde{\gamma}}w_e \le \min\{\frac{1}{4}R,\ \frac{1}{4}r^\flat\}. \tag{5.15}$$

Put $\varphi \equiv -1$ for the states $x_0 \in X(\overline{\alpha})$ with $x_{01} \ge 0$. Using (5.11), (5.13) and (5.15) and taking into account the estimate

$$\dot{x}_1 = \frac{w^{(1)}}{R}x_2 + v_1 \ge v_1 \ge -w_e,$$

we obtain that any trajectory emanated from the points x_0 arrives at the axis x_1 within the time $\overline{\alpha}/\widetilde{\gamma}$. Besides, the trajectory remains on the right side from the vertical straight line $x_1 = \max\{-R/4,\ -r^\flat/4\}$.

Similarly, setting $\varphi = 1$ and using (5.12), (5.14) and (5.15), one obtains that any trajectory emanated from the points $x_0 \in X(\overline{\alpha}), x_{10} \le 0$, arrives at the axis x_1 within the time $\overline{\alpha}/\widetilde{\gamma}$. Besides, the trajectories remain on the left side from the straight line $x_1 = \min\{R/4,\ r^\flat/4\}$.

Thus player P can bring trajectories to the axis x_1 from any initial point x that belongs to the strip $X(\overline{\alpha})$. It follows from this property that $\hat{C}_U \bigcap X(\overline{\alpha}) = \emptyset$. Moreover, there is no any collection of v-stable sets that monotonically expands from the set $\hat{C}_U$ and fills out the whole plane. Indeed, let us suppose the opposite. Denote by $\bar{S}$ the smallest of v-stable sets that has common points with $X(\overline{\alpha})$. Then player E, using the discrimination of player P, can keep trajectories in $\bar{S}$ for infinite time. On the other hand, player P, applying a constant control, can bring trajectories to

the axis x_1 from any point of the set $\bar{S} \bigcap X(\overline{\alpha})$ within a finite time that is he can bring out trajectories from the v-stable set $\bar{S}$. We come to a contradiction.

The considerations of this section make clear that it is impossible to obtain examples with holes in the solvability sets for the classical game. For this reason, the acoustic game is of particular interest.

6. Analysis of Computation Results

We compute the level sets of the value function. The optimal time for a given state x is the minimal time τ subject to $x \in W(\tau, M)$.

We have not a priori estimates of the accuracy of the algorithm. The correctness of computations is verified via comparison of computation results with the qualitative results of [10], [19] and [20]. Additionally, the correctness of the construction of barriers is checked and the fronts behavior after the termination of barriers is inspected. An analytical description of fronts is absent for the examples considered.

In the following sections 6.1–6.3, the results of computing the sets $W(\tau, M)$, $\tau = i\Delta$, for the problems from sections 2.1–2.3 are discussed. The computation step Δ in the examples below is selected experimentally. For some examples of section 6.1, a smaller time step than the one for sections 6.2 and 6.3 is required to find out all fine details of the evolution of the fronts. The time step depends also on the size of the terminal set M and on the length of the reverse time interval considered.

For many examples given below, three-dimensional graphs of the value function are presented together with the computed fronts. The programs for the visualization of such graphs were developed by Averbukh and Pykhteev [2].

6.1. *Level sets of the value function in the homicidal chauffeur game*

In Figure 25, the computation results for the following values of parameters are presented: $w^{(1)} = 3$, $w^{(2)} = 1$ and $R = 3$. The set Q is a 25-polygon inscribed into the circle of radius $w^{(2)}$ with the center at $(0, 0)$. The terminal set M is a 15-polygon approximating the circle of radius $l = 1$ with the center at the origin. The step Δ is 0.01. Every 10th front is plotted. The fronts are symmetric with respect to the x_2-axis. The left and right barrier lines terminate on the lower boundary of the sets A and B, respectively. After that, the left and right ends of the front begin to bend round the left and right barrier lines, and two symmetric corner points arise on the front. These corner points become more and more close, and at $\tau = 8.42$, a self-intersection of the front occurs. As a result, the front is divided into two parts: the internal part and the external one. The computations are carried out from each part separately. The internal part of the front propagates upwards sliding with its ends along the corresponding barriers. At $\tau = 10.6$, it collides with the terminal set, and two symmetric gaps which are filled out at $\tau = 11.3$ arise. The external part of the front propagates outwards and can fill out the whole plane with the time (the last external front in the picture corresponds to $\tau = 9$). Therefore, for each point of the plane, the minimal guaranteed time of approaching the set M is finite. For the points where the value function coincides with the function of programming maxmin, the optimal guaranteed time can be computed analytically. Our results are in a good agreement with the values given for some particular points in [26].

In Figure 26, a three-dimensional graph of the value function of Figure 25 example is presented. The axes in the horizontal plane are x_1 and x_2, and the vertical axis measures the value function. The picture shows the value function for the region of (x_1, x_2) where the fronts are computed. The change of color from red to violet corresponds to the increase of function values.

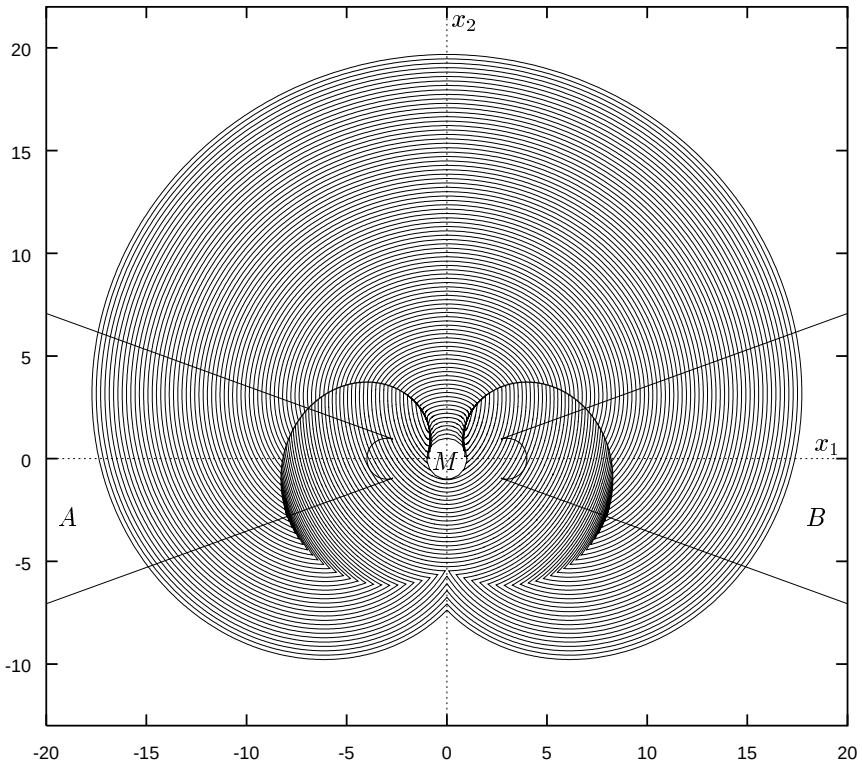

Fig. 25. Level sets of the homicidal chauffeur game for $w^{(1)} = 3$, $w^{(2)} = 1$ and $R = 3$.

For two examples shown in Figures 27 and 30, the following values of parameters of the problem are used: $w^{(1)} = 2$, $w^{(2)} = 0.6$, $R = 0.2$. The set Q is a 25-polygon inscribed into the circle of radius $w^{(2)}$ with the center at $(0, 0)$. The set M is a regular polygon inscribed into the circle of radius 0.015. The center of the circle is $(0.2, 0.3)$ and $(0, -0.45)$ for Figures 27 and 30, respectively. The step Δ is 0.001. The sets $W(8k\Delta, M)$, $k = 1, 2, ...$, are depicted.

Let us explain the constructions presented in Figure 27. The right barrier line terminates on the lower boundary of the auxiliary set B. The front begins to bend round this barrier line. After some time, the left barrier line ends on the lower boundary of the set A, and the left part of the front bends round the left barrier. The left and the right parts of the front go towards one to other till the first self-intersection of the front occurs at $\tau = 0.725$. The front is divided into two parts (internal and external). For $\tau > 0.725$, only internal fronts that propagate into the

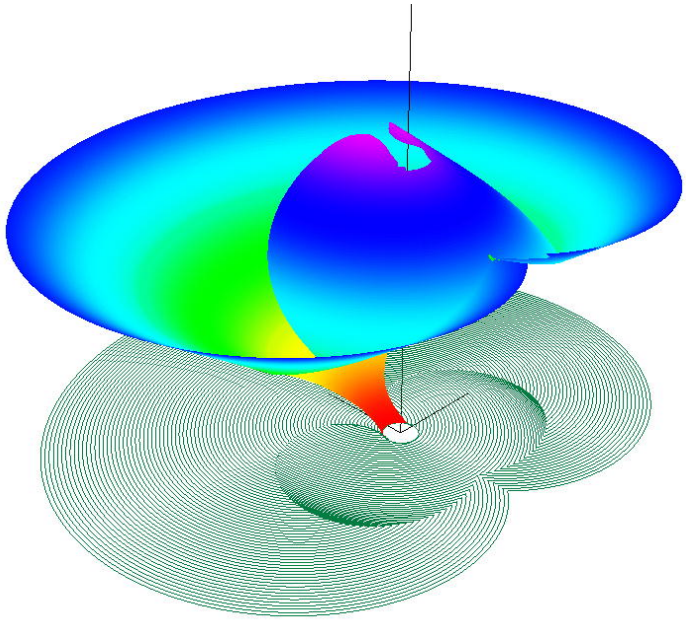

Fig. 26. The graph of the value function for $w^{(1)} = 3$, $w^{(2)} = 1$ and $R = 3$.

"region of turn" are drawn. Here, very complicated structure of fronts arises.

At $\tau = 0.904$, the second self-intersection of the front which is drawn with the thick dash line produces two gaps that are filled out afterwards separately. The next front consists of three parts: an exterior part (which is not shown), and two interior parts (two loops inside the dash contour). The greatest value of τ in the region of turn is 0.95. This corresponds to the time when the fronts complete filling the gap on the left hand side of the axis x_2. The gap with the center on the axis x_2 is filled at $\tau = 0.948$. As a result, the sets $W(\tau, M)$ for $0.904 < \tau < 0.948$ are triply connected.

Figures 28 and 29 show three-dimensional graphs of the value function corresponding to the level sets of Figure 27. Two different points of view were used. In Figure 29, level lines of the value function are additionally plotted onto the graph.

In Figure 30, the fronts are symmetric with respect to the x_2-axis. The self-intersection of the front occurs at $\tau = 0.355$. The gap which arises after $\tau = 0.355$ and whose center has coordinates $(0, 0.22)$ is filled out with level lines separately. Filling out the gap finishes at $\tau = 0.38$. The sets $W(\tau, M)$ for $0.355 < \tau < 0.38$ are doubly connected. At $\tau = 0.766$, the front collides with the barrier lines. Two symmetric gaps arise. The structure of the fronts within the right gap is shown in an enlarged scale in Figure 31a. Filling out the gap ends at $\tau = 0.85$. The sets $W(\tau, M)$, $0.766 < \tau < 0.85$, are triply connected. The computation are carried out up to $\tau = 0.872$. The value function is discontinuous on two symmetric barrier lines that emerge tangentially from the boundary of M and terminate on the upper

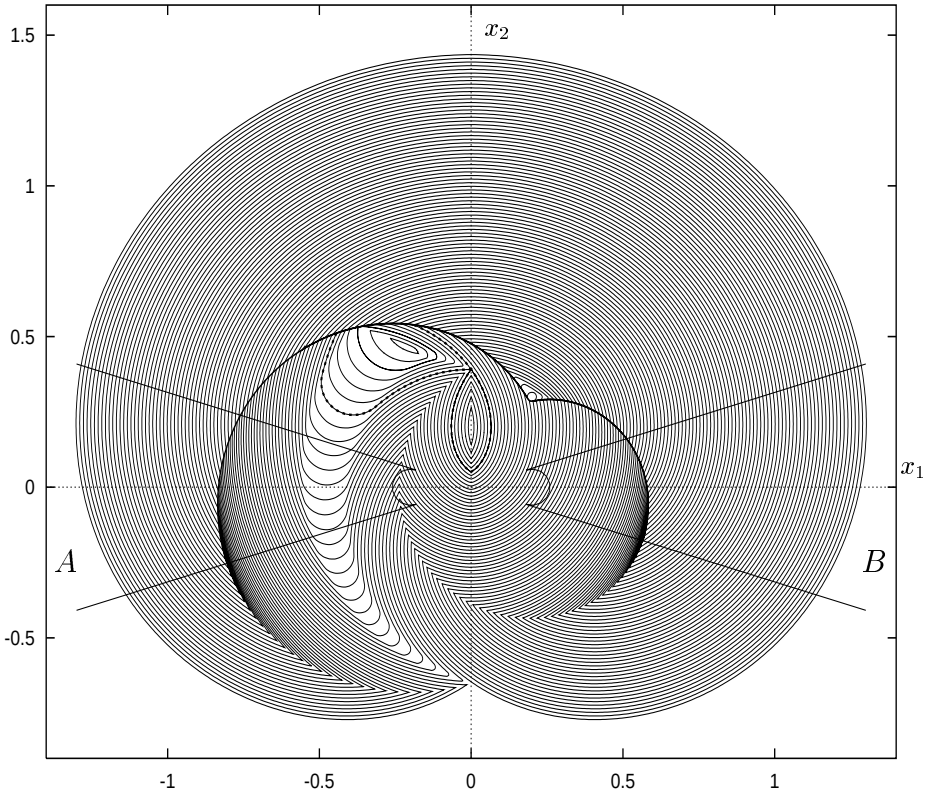

Fig. 27. Complicated structure of level sets in the "region of turn." The terminal set is a small circle in the first quadrant; $w^{(1)} = 2$, $w^{(2)} = 0.6$ and $R = 0.2$.

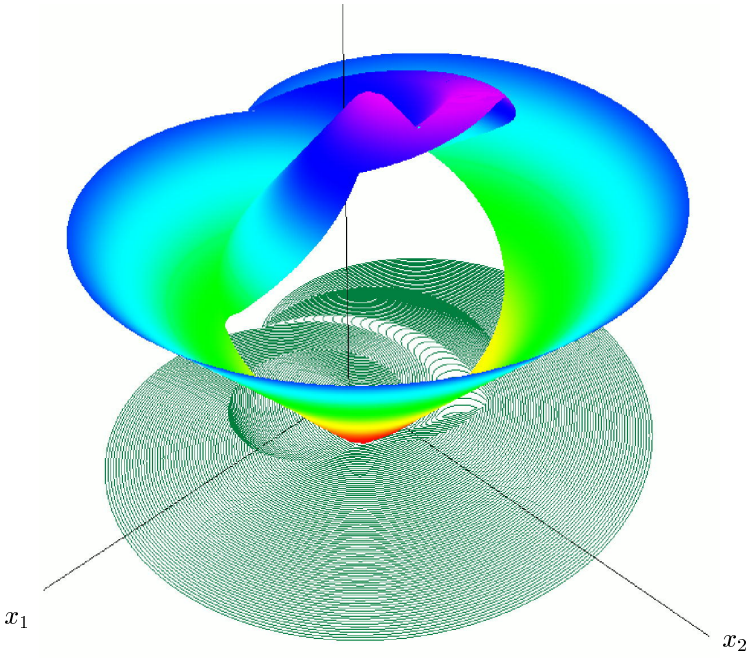

Fig. 28. The graph of the value function for level sets in Figure 27.

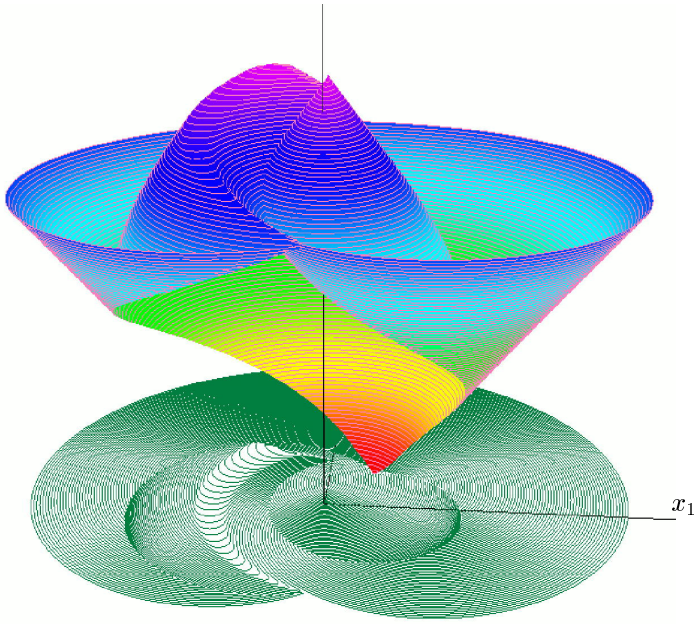

Fig. 29. The graph of the value function from another point of view.

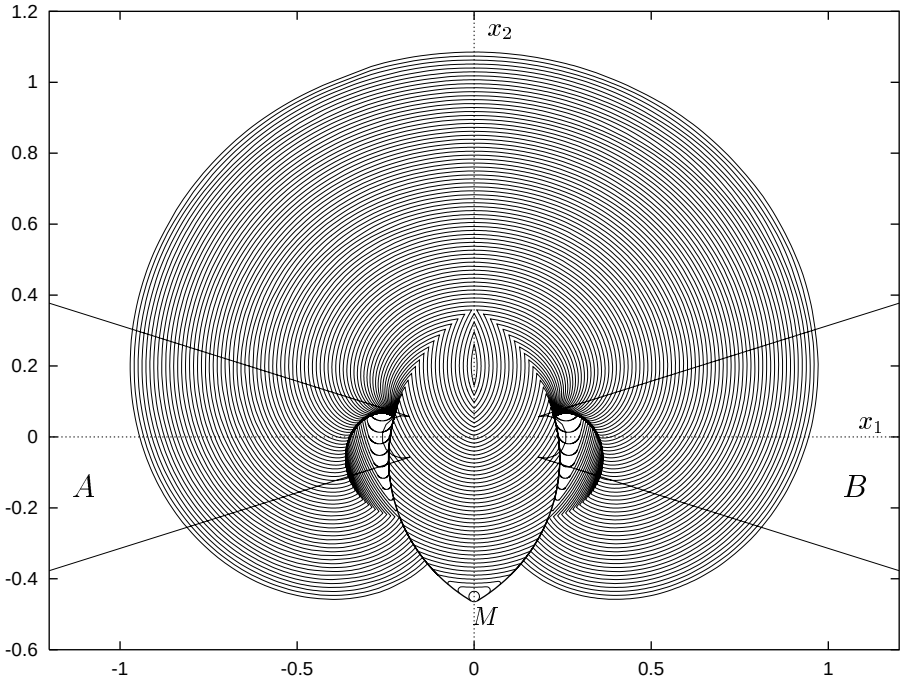

Fig. 30. Level sets of the value function for $w^{(1)} = 2$, $w^{(2)} = 0.6$, $R = 0.2$ and the terminal set with the center on x_2-axis.

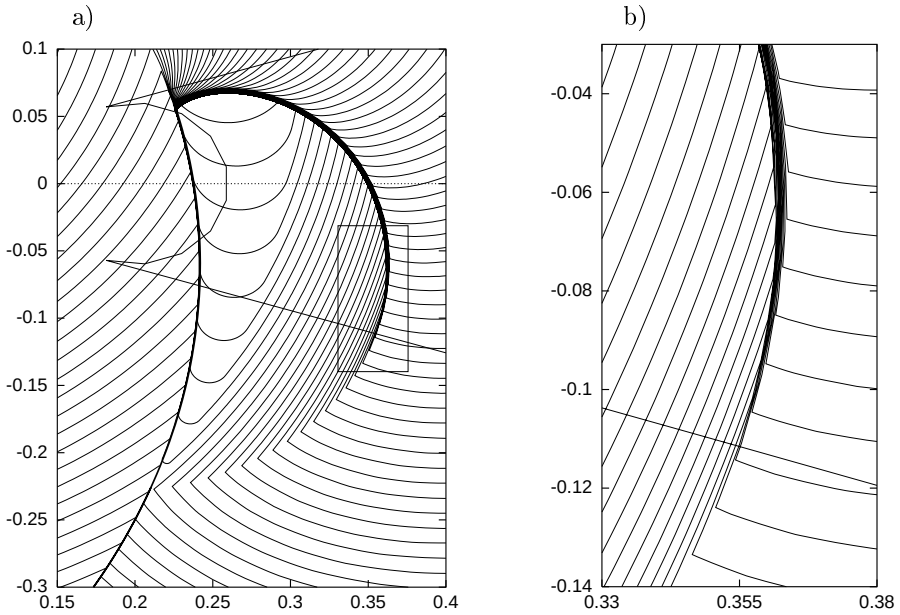

Fig. 31. Enlarged fragments of Figure 30.

boundaries of the auxiliary sets A and B. In regions of the accumulation of fronts, the value function changes very rapidly but it is continuous. Figure 31b shows an enlargement of the accumulation region within the rectangle in Figure 31a.

Let us explain more precisely what happens when fronts begin to bend round the accumulation region. After coming the front onto the lower boundary of the set B, a new corner point $k(\tau)$ arises on the front (see Figure 32a). The point $k(\tau)$ moves up as τ increases. The point $b(\tau)$ of the front moves down along the outer side of the barrier line dg at a low rate. The part of the front between the points $b(\tau)$ and $k(\tau)$ propagates to the outside very slowly. The length of the curve $b(\tau)k(\tau)$ becomes smaller as τ increases. The part of the front between the points $k(\tau)$ and $c(\tau)$ moves enough rapidly to the left, and the front collides with the barrier line dg at $\tau = 0.766$.

It is useful to compare this evolution of fronts with that one in Figure 27 where the ends of the front move down along the corresponding barrier lines and then bend round them. In Figure 32b, the bending of the right barrier line is shown. Here, the point $k(\tau)$ is the endpoint of the front. It moves up along the outer side of the barrier line fe.

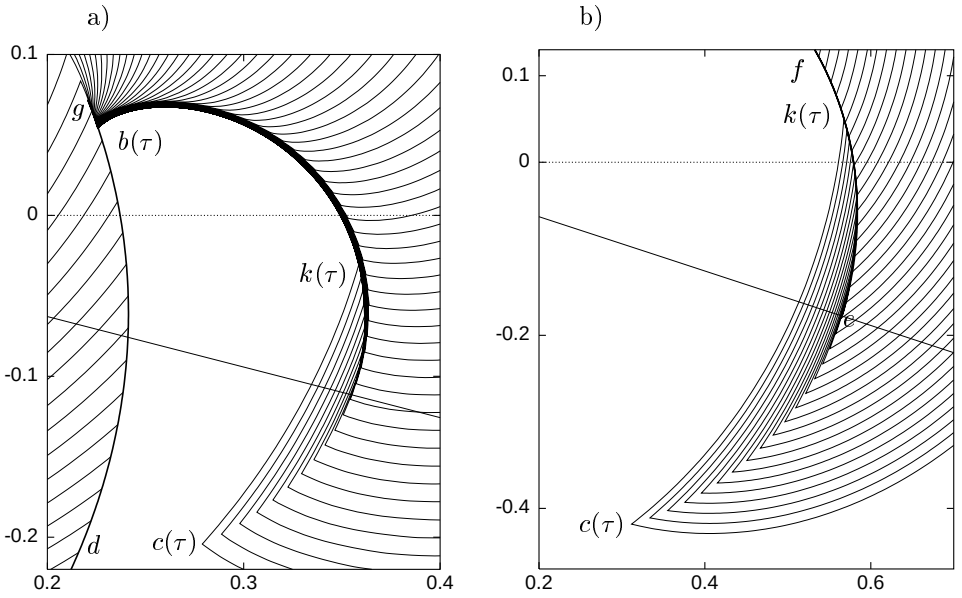

Fig. 32. The evolution of fronts in regions of continuous and discontinuous change of the value function.

For the example in Figure 33, the following values of parameters are used: $w^{(1)} = 2$ and $R = 0.2$. The terminal set M is a regular 25-polygon inscribed into the circle of the radius 0.015 with the center at $(0.2, -0.4)$. The set Q is the triangle with the vertices $(-0.96, 0.8)$, $(0.96, 0.8)$ and $(0, -4.8)$. The step Δ is 0.001. The sets $W(20k\Delta, M)$, $k = 1, 2, ...$, are depicted. In this example, the left barrier line finishes

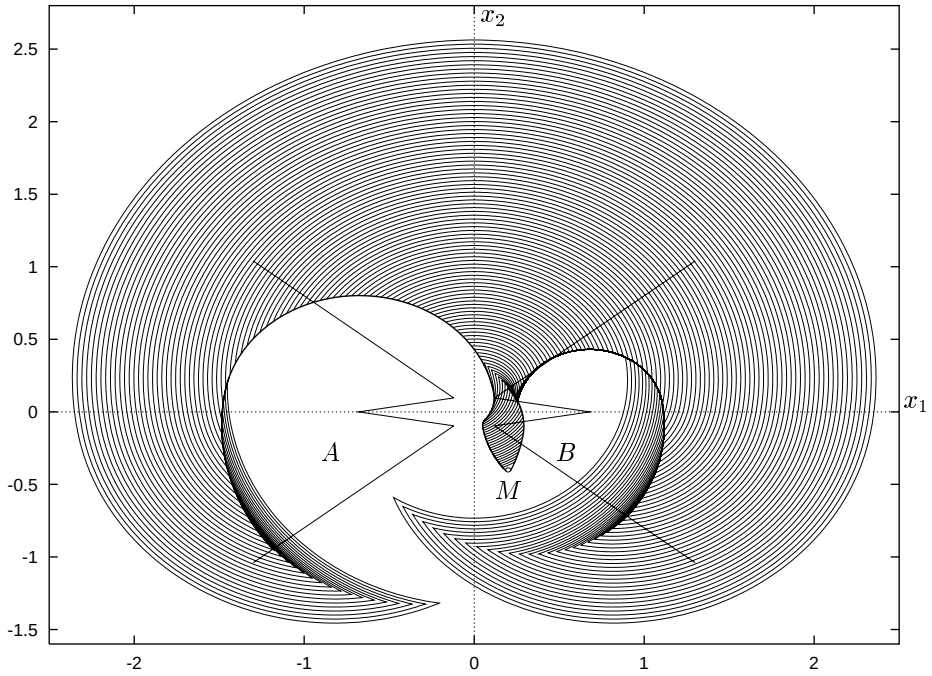

Fig. 33. Level sets of the value function for $w^{(1)} = 2$, $R = 0.2$ and a triangular constraint Q of player E.

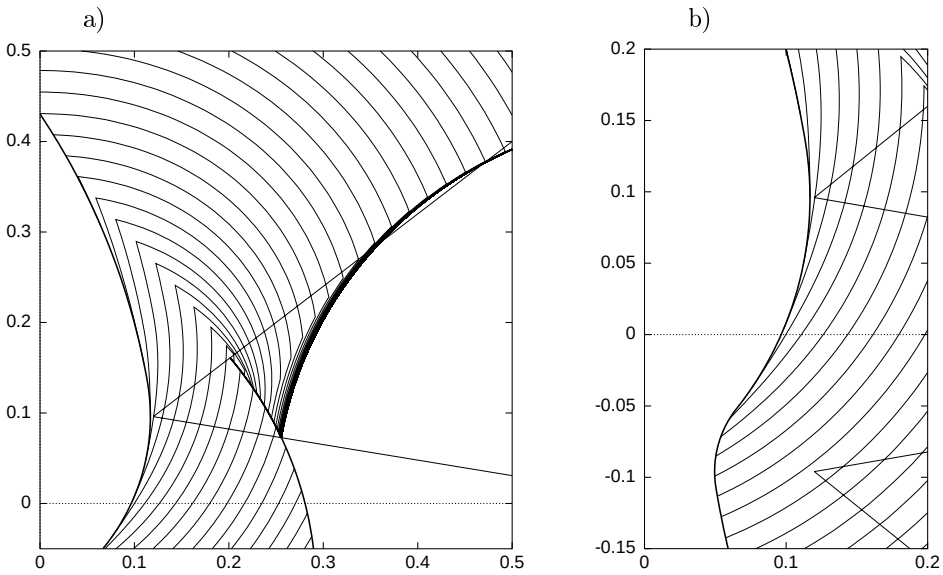

Fig. 34. Enlarged fragments of Figure 33.

on the lower part of the boundary of the set A, and the right barrier line finishes on the upper part of the boundary of the set B. The structure of fronts near the end of the right barrier line is shown in Figure 34a. The accumulation of fronts means very rapid changing the value function. The twisted part of the left barrier line is depicted in Figure 34b.

Figure 35 shows a three-dimensional graph of the value function corresponding to Figure 33 example.

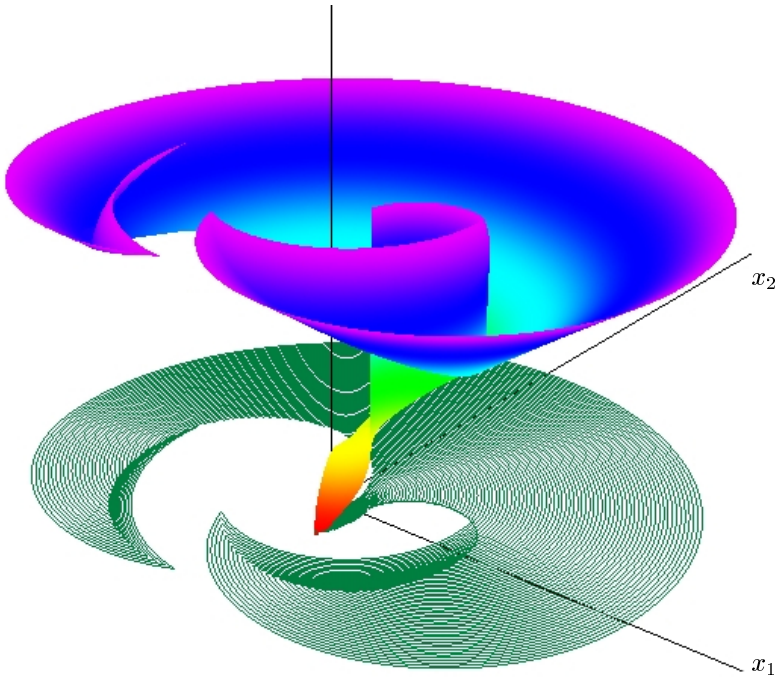

Fig. 35. The graph of the value function for level sets in Figure 33.

In all examples presented in this section, the barriers finish on the boundaries of the auxiliary sets A and B. This is consistent with the fact that every barrier line is a smooth semipermeable curve of one of the families described in section 4, or it is composed of such smooth semipermeable curves. All of the barriers that were constructed approximate corresponding semipermeable curves very good.

The correctness of the computation of level sets of the value function can be additionally verified using the information about the solvability set of the game of kind. Very often, the solvability set is determined by a system of semipermeable curves of the first and second type which is generated by the terminal set. We explain using the example from Figure 33 how such a system can be constructed. The semipermeable curves $p^{(2),1} \in \Lambda^{(2),1}$ and $p^{(1),2} \in \Lambda^{(1),2}$ emanated in reverse time from the endpoints of the usable part of M do not intersect each other before they terminate on the boundaries of the corresponding domains (Figure 36). The join of $p^{(2),1}$ and

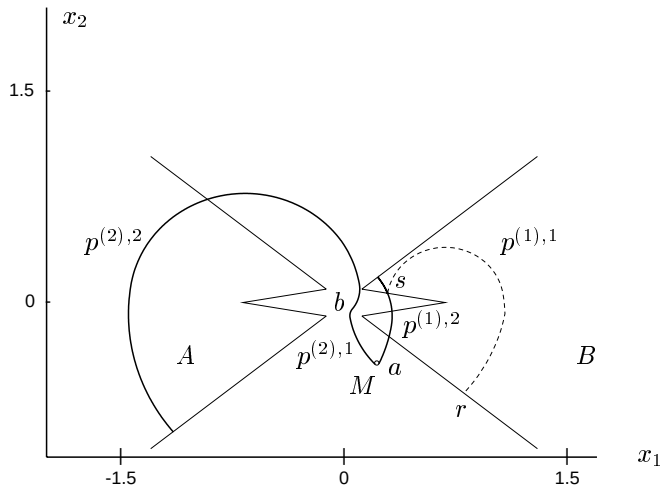

Fig. 36. The system of semipermeable curves for the example with the triangle set Q.

$p^{(2),2}$ at the point b is smooth. This provides the semipermeability property of the composite semipermeable curve $p^{(2),1} \bigcup p^{(2),2}$ at b. The curve $p^{(2),1} \bigcup p^{(2),2}$ does not intersect $p^{(1),2}$. Though the join of the arc $as \subset p^{(1),2}$ and the curve $p^{(1),1}$ is non-smooth, the semipermeability property is fulfilled (see [21]–[23] and [32] for analogous situations) at the junction point s. Thus the curve asr is a composite semipermeable curve of the first type. The composite semipermeable curves of the first and second types do not intersect each other. Further semipermeable curves are not being produced. One can prove using the described mutual disposition of the semipermeable curves that the solvability set of the game of kind is the whole plane. Numerical computation of the level sets of the value function confirms this fact.

One can see that the curve $p^{(2),1} \bigcup p^{(2),2}$ is the left barrier line in Figure 33. The curve $p^{(1),2}$ is the right barrier. It is interesting to observe that the curve $p^{(1),1}$ is not a barrier. The value function is continuous across this curve. Since asr is a composite semipermeable curve, the fronts can not penetrate the curve $p^{(1),1}$ from above. Therefore, the arcs of the fronts that form the accumulation region in Figure 34a should remain above the curve $p^{(1),1}$. The fulfillment of this property for computed fronts can be considered as an additional confirmation of the algorithm validity.

A similar location of the accumulation region of fronts can be established for the example in Figure 30.

6.2. *Level sets of the value function in the acoustic game*

The examples of this section correspond to $w^{(1)} = 1$, $R = 0.8$ and $s = 0.75$. The terminal set M is the rectangle $\{(x_1, x_2) \in R^2 : -3.5 \leq x_1 \leq 3.5,\ -0.2 \leq x_2 \leq 0\}$. The set Q is a circle of radius w_e. The constraint $\mathcal{Q}(x)$ is a circle of radius $\min\{|x|,\ s\}w_e/s$ which is approximated by a polygon. Below, the dependence of the solution of the acoustic game on the parameter w_e is demonstrated.

In Figure 37, the initial computations for $w_e = 0.4$ are shown. The step Δ is 0.005. The usable part of the terminal set M consists of three segments: the upper side of M and two segments on the lower side. The upper fronts that occur until $\tau = 0.29$ are bounded on the left and right by barrier lines. At $\tau = 0.29$, these barrier lines meet the upper boundaries of the sets A and B, so they terminate. The value function is discontinuous across the barrier lines. For $\tau > 0.29$, the fronts begin to envelop the barrier lines, and left and right corner points on the upper front arise. The propagation of the front beyond the barrier lines from these corner points is at a very low rate. An enlargement of this development of the fronts on the right hand side is presented in Figure 38.

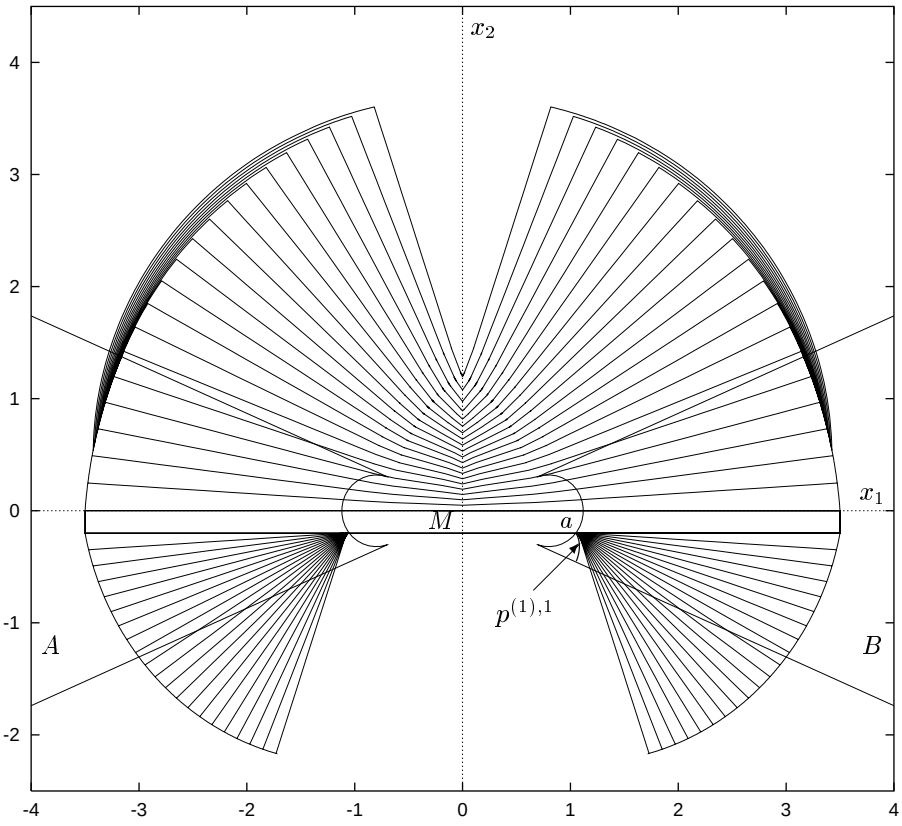

Fig. 37. Level sets for $w_e = 0.4$; 200 upper and lower fronts, every 10th front is plotted.

The continuation of the computation is shown in Figure 39. The upper and lower fronts are calculated until $\tau = 1.6$ and $\tau = 3.3$, respectively. The left and right lower fronts collide at $\tau = 1.76$. Only one lower front remains after this collision. The greatest value of τ below M occurs on the lower boundary of M at the point $(0, -0.2)$.

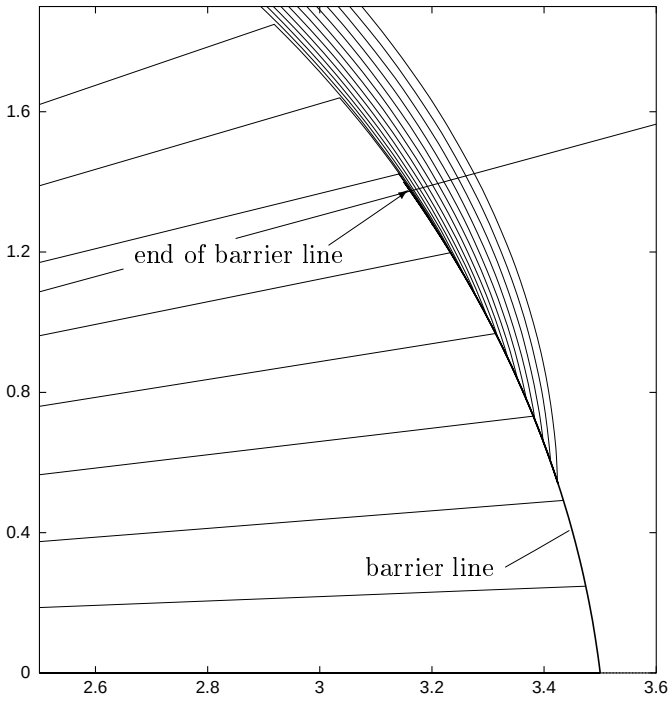

Fig. 38. The structure of fronts near the barrier line.

An enlargement of the accumulation of the lower fronts is shown in Figure 40. We see that the end of the front moves along the terminal set from the end of the usable part to the point a on the boundary of the set B. The accumulation of fronts begins when they approach the semipermeable curve $p^{(1),1}$ that emanates from the point a, as shown in Figure 37. The value function changes very rapidly in the accumulation region, but it remains continuous.

In Figures 41 and 42, three-dimensional graphs of the value function for this example are presented. Two different points of view were used. In Figure 42, level lines of the value function are additionally plotted onto the graph. Remind that the change of color from red to violet corresponds to the increase of function values.

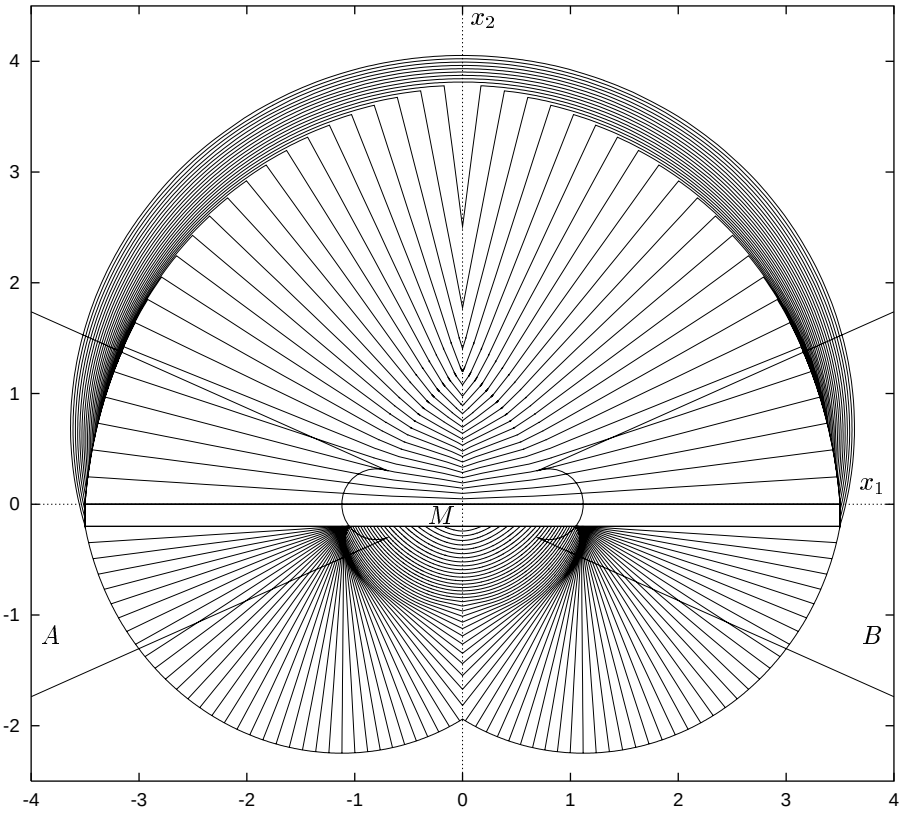

Fig. 39. Level sets for $w_e = 0.4$; 320 upper fronts, 660 lower fronts.

Figure 43 presents the computation results for $w_e = 0.95$ and $\Delta = 0.005$. As in the previous example, the upper barrier lines end at some moment of reverse time, and the fronts begin to envelop them. The main difference from before is the formation of a loop where the upper fronts from the two sides of the figure meet. In this example, the region within this loop (a "lagoon") is filled out entirely by the further development of the fronts, the filling out being completed at $\tau = 1.68$.

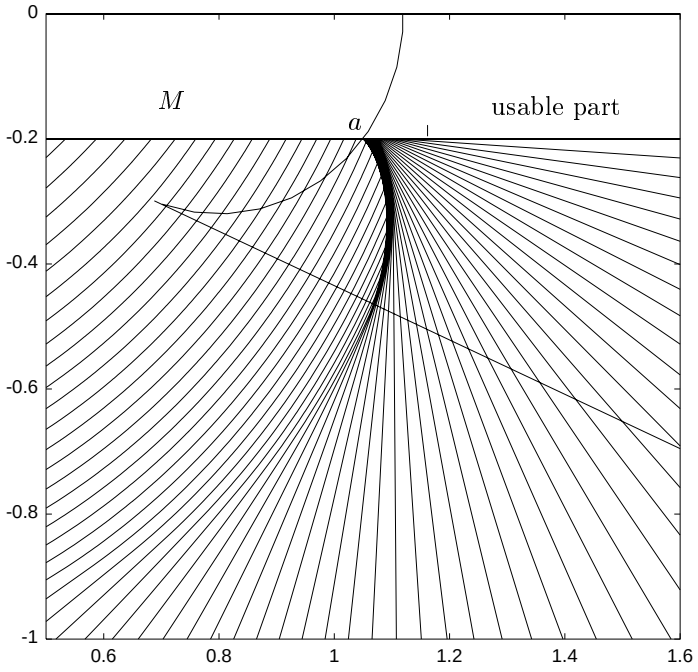

Fig. 40. The accumulation of fronts near the point a.

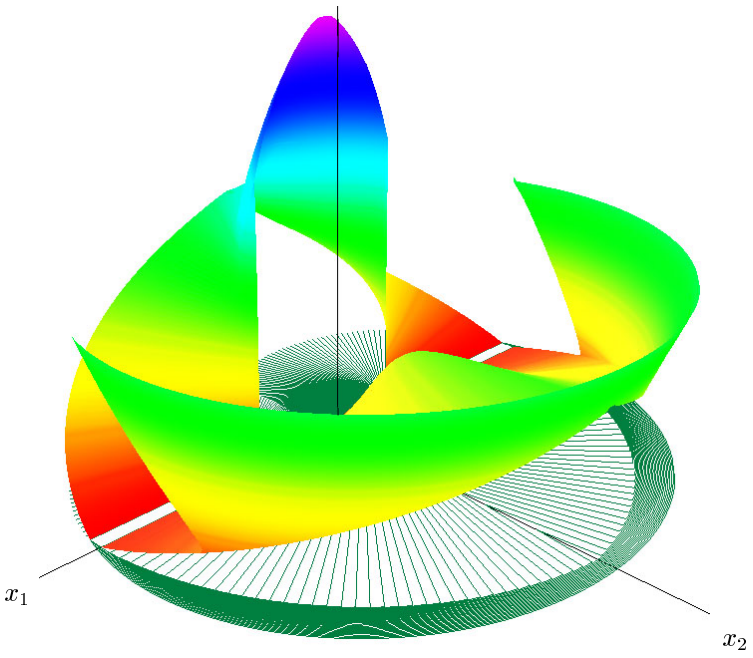

Fig. 41. The graph of the value function for level sets in Figure 40; $w_e = 0.4$.

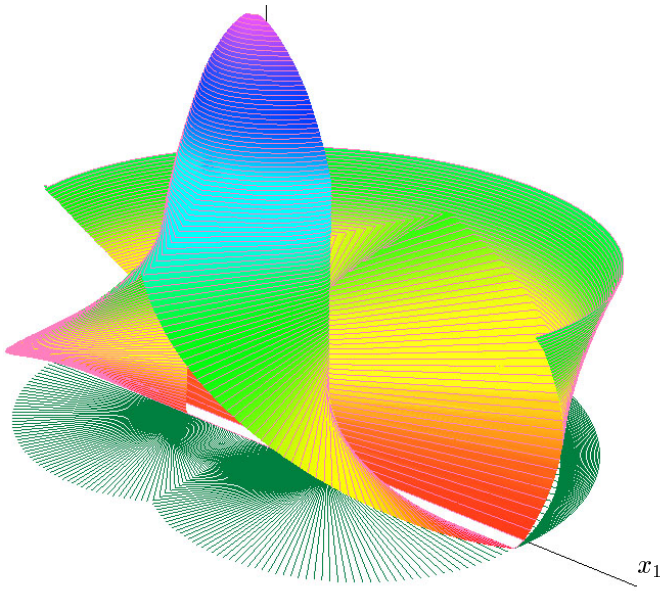

Fig. 42. The graph of the value function (with plotted level lines) for $w_e = 0.4$ from another point of view.

An important feature of the lower part of Figure 43 is that the semipermeable curve $p^{(1),1}$, emanating from the point a, intersects the right barrier which is the semipermeable curve $p^{(2),1}$. This did not happen in the previous example. Thus the right lower fronts are confined to the right side of the curve $p^{(1),1}$. The time of attaining the terminal set becomes infinite as the fronts approach the curve $p^{(1),1}$. A symmetric situation occurs for the left lower fronts. All the fronts are computed until $\tau = 2.4$.

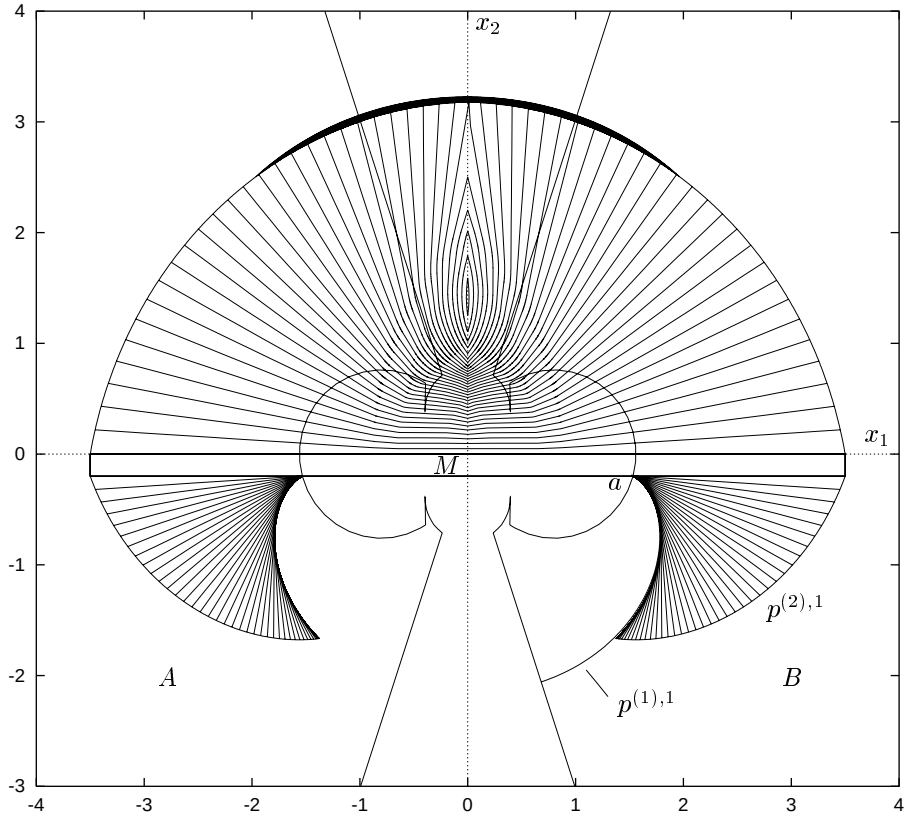

Fig. 43. Level sets for $w_e = 0.95$; 480 upper and lower fronts, every 10th front is plotted.

Figure 44 shows the computation results for $w_e = 1.1$ and $\Delta = 0.0025$. The structure of the fronts is similar to that in Figure 43. The main difference is that the upper barrier lines intersect on the vertical axis at $\tau = 1.495$, and further computation of upper fronts is being done within the lagoon only. The computation is done until the time $\tau = 2.0675$ when the lagoon is completely filled out.

The corresponding graphs of the value function for two different points of view are given in Figures 45 and 46. In Figure 46, level lines of the value function are additionally plotted onto the graph.

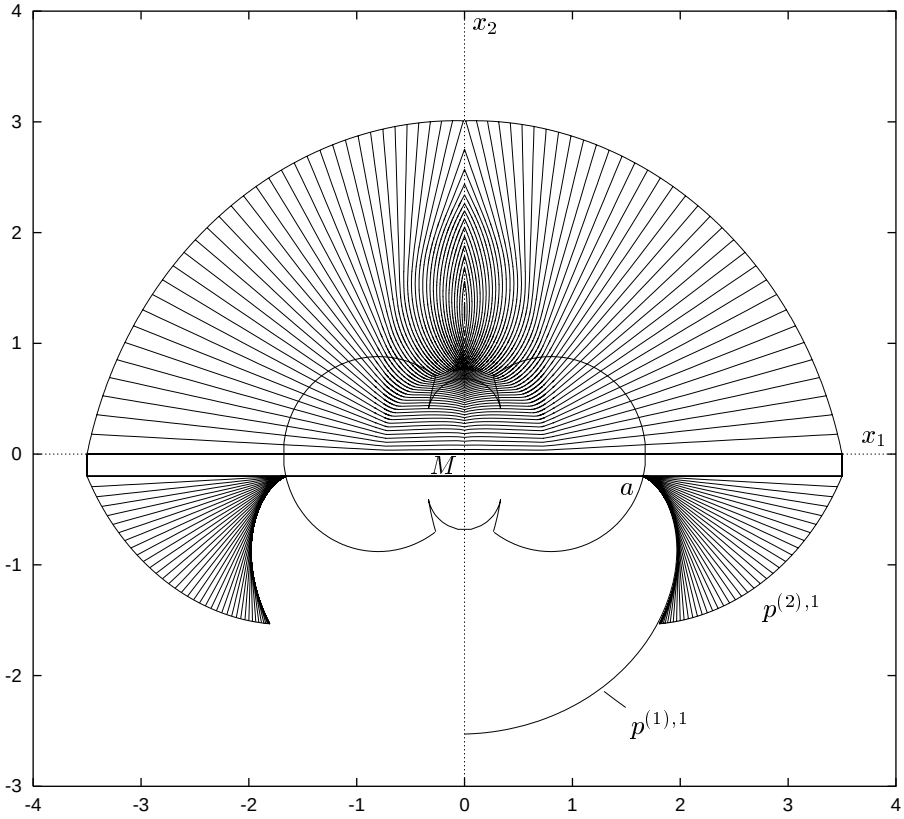

Fig. 44. Level sets for $w_e = 1.1$; 827 upper and lower fronts, every 17th front is plotted.

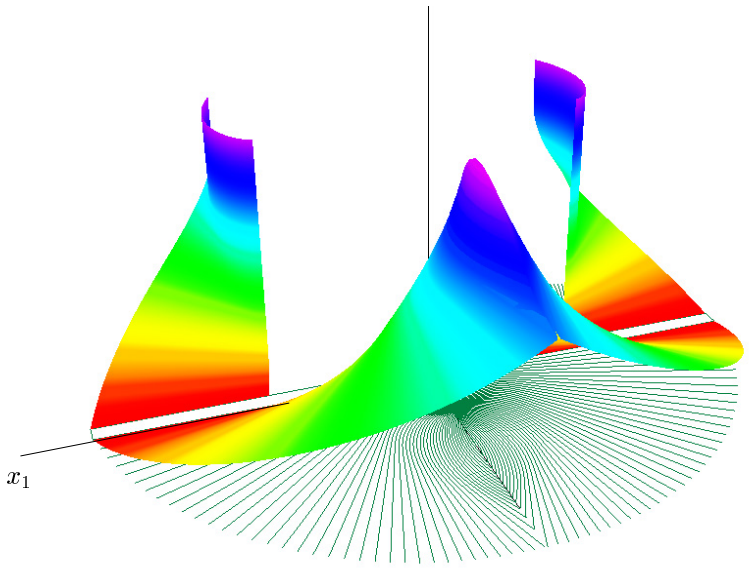

Fig. 45. The graph of the value function for level sets in Figure 44; $w_e = 1.1$.

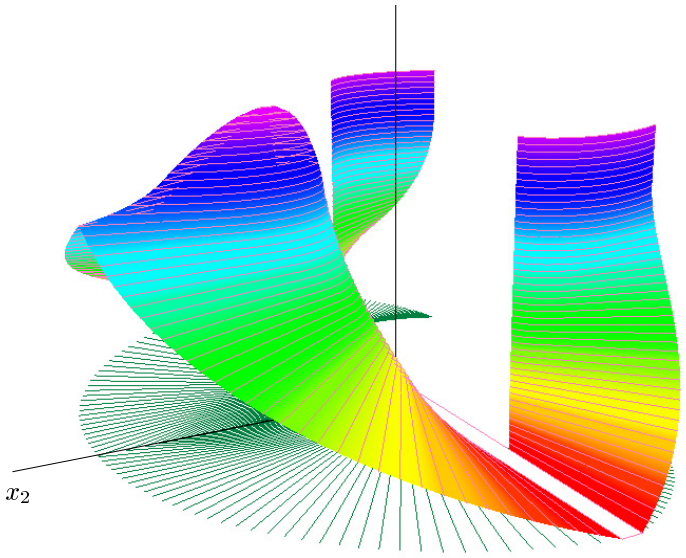

Fig. 46. The graph of the value function (with plotted level lines) for $w_e = 1.1$ from another point of view.

The following facts were found experimentally. A lagoon is generated by the upper fronts only if $w_e \geq 0.65$. For $w_e \in [0.65, 1.37)$, a lagoon occurs and is completely filled by the further development of the fronts. For $w_e \in [1.37, 1.61]$, the fronts do not fill the lagoon completely. For $w_e > 1.61$, the lagoon disappears.

Figure 47 presents computational results for $w_e = 1.5$ and $\Delta = 0.005$. The left and right parts of the upper front meet at $\tau = 2.855$. Then the computation within the lagoon begins. The fronts do not penetrate the set $\hat{C}_U$, which is a hole inside the solvability set of player P, the value function being infinite for $x \in \hat{C}_U$. The computation is done until $\tau = 3.73$. The structure of the lower fronts is similar to that in the previous example.

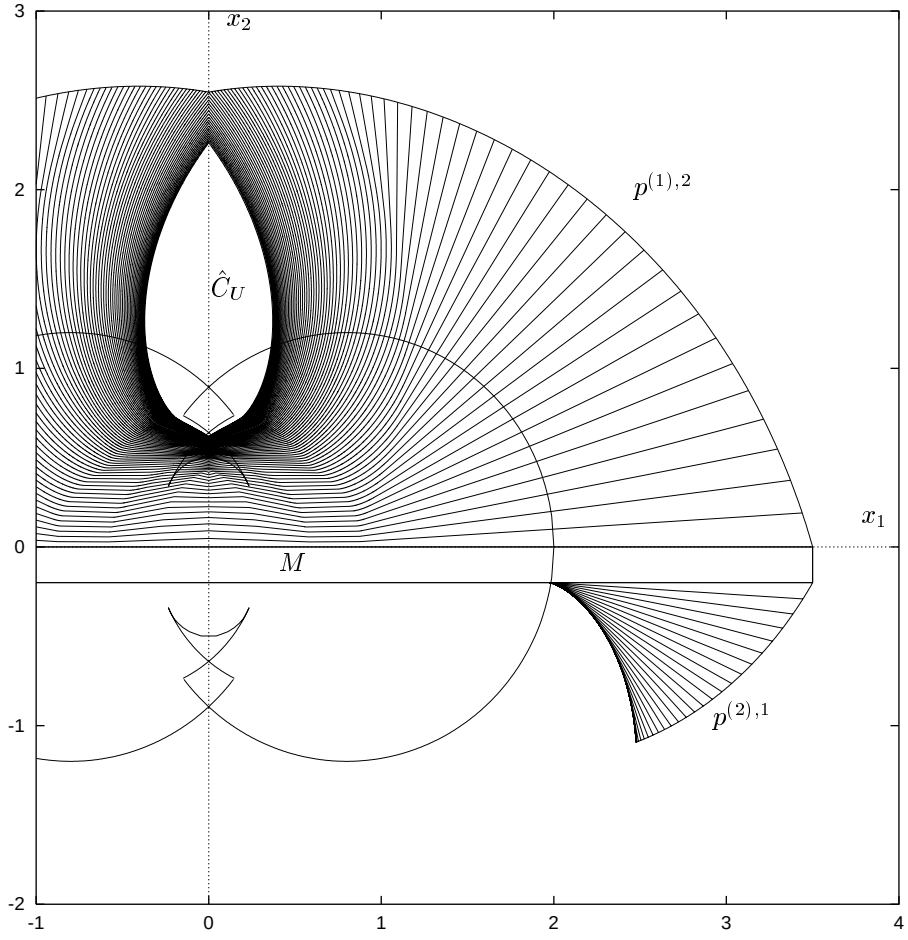

Fig. 47. Level sets for $w_e = 1.5$; 746 upper fronts, 340 lower fronts, every 10th front is plotted.

In Figure 48, a three-dimensional graph of the value function of Figure 47 example is presented.

Further increases in the value of w_e extend the set $\hat{C}_U$. For example, Figure 49 gives computational results for $w_e = 1.9$ and $\Delta = 0.01$. The upper and lower fronts are computed until $\tau = 8.42$ and $\tau = 1.6$, respectively. The graphs of the value function for two different points of view are shown in Figures 50 and 51.

We have studied the dependence of the solution on the parameter w_e. In Figure 52, one more variant of solution is presented for the following values of parameters: $w^{(1)} = 1$, $w_e = 1.4$, $R = 0.3$, $s = 0.75$ and $\Delta = 0.01$. The structure of upper fronts is similar to that in Figure 44. A hole in the lower part of the picture occurs because the lower fronts are confined to the right side of the curve $p^{(1),1}$ and to the left side of the curve $p^{(2),2}$ which is symmetric to $p^{(1),1}$ with respect to the axis x_2. The appearance of the hole here is not connected with the superiority sets. The lower fronts are computed till $\tau = 9$. The computation of the upper fronts ends at $\tau = 1.64$.

Figures 53 and 54 show graphs of the value function of Figure 52 example. Two different points of view were used. The top of the graph corresponds to $\tau = 4.75$.

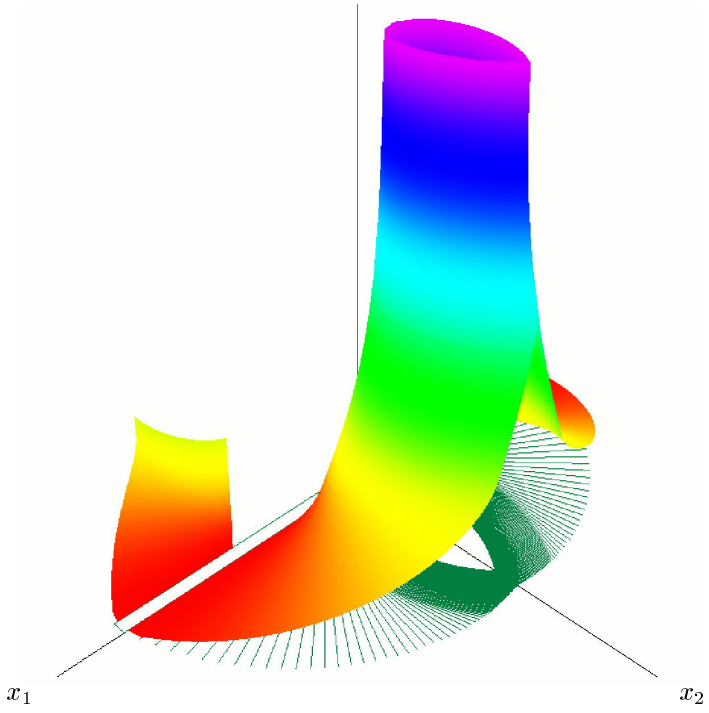

Fig. 48. The graph of the value function for level sets in Figure 47; $w_e = 1.5$.

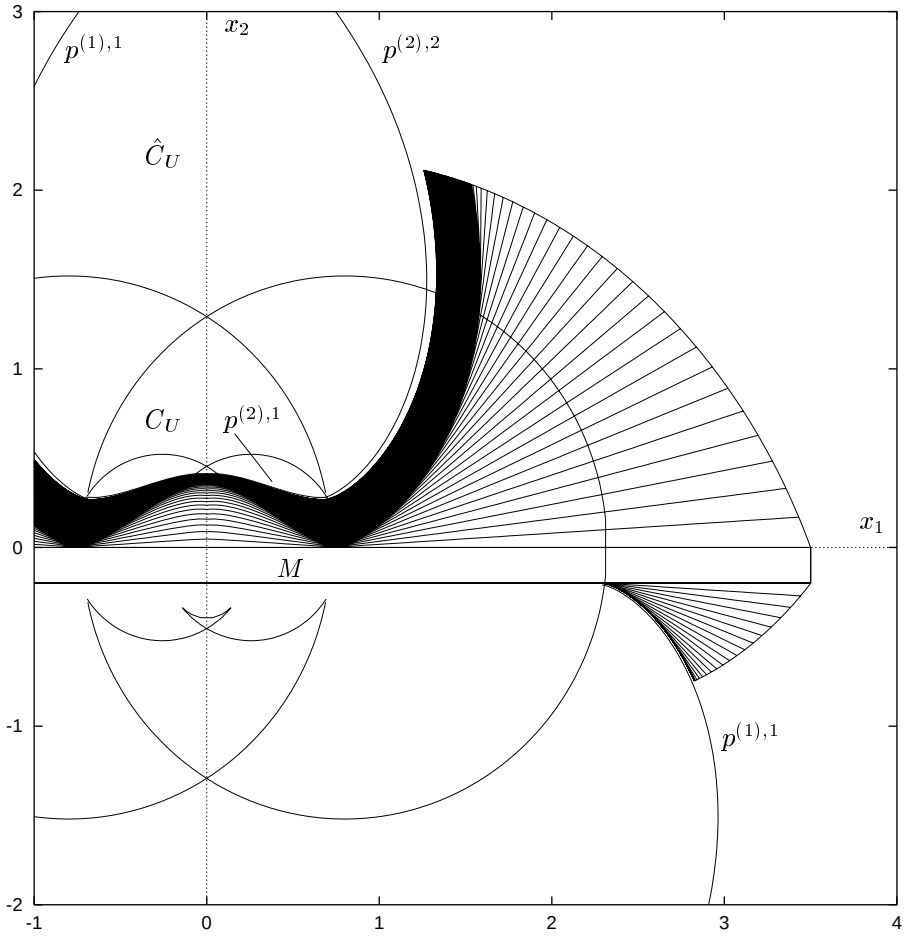

Fig. 49. Level sets for $w_e = 1.9$; 842 upper fronts, 160 lower fronts, every 5th front is plotted.

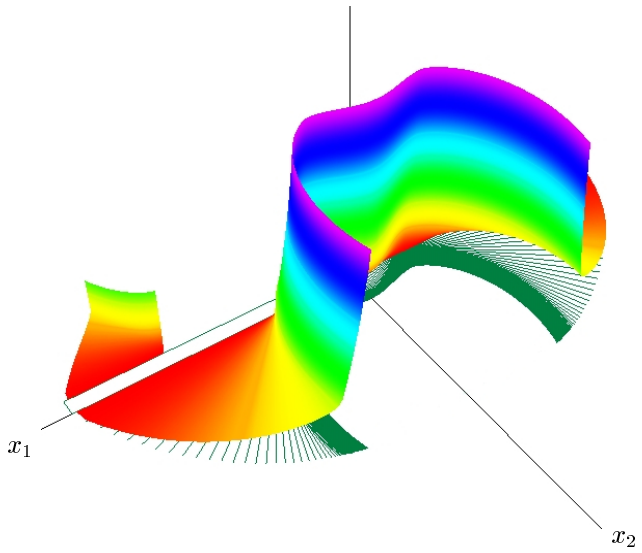

Fig. 50. The graph of the value function for level sets in Fugure 49; $w_e = 1.9$.

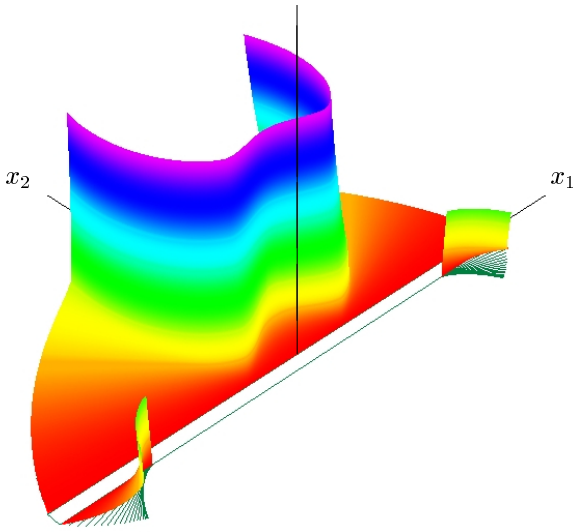

Fig. 51. The graph of the value function for $w_e = 1.9$ from another point of view.

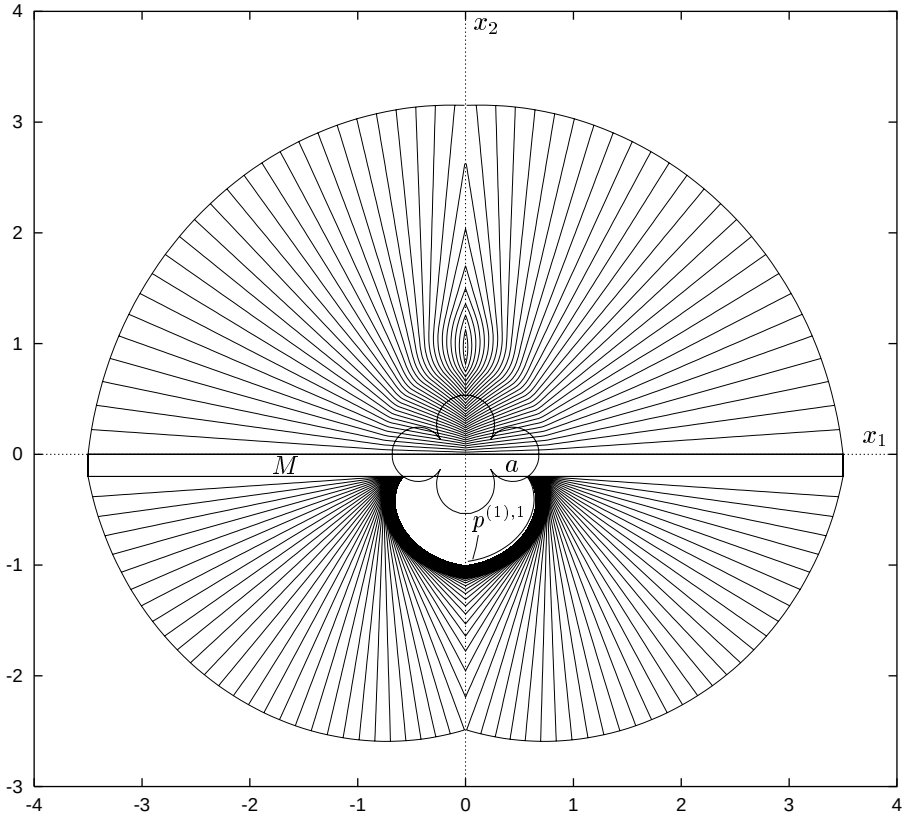

Fig. 52. Level sets for $w_e = 1.4$, $R = 0.3$; 164 upper fronts and 900 lower fronts, every 5th front is plotted.

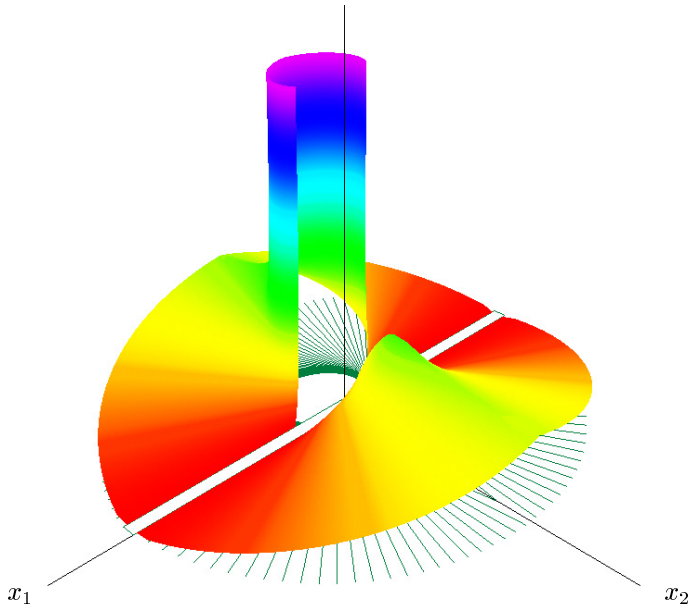

Fig. 53. The graph of the value function for level sets in Figure 52; $w_e = 1.4$, $R = 0.3$.

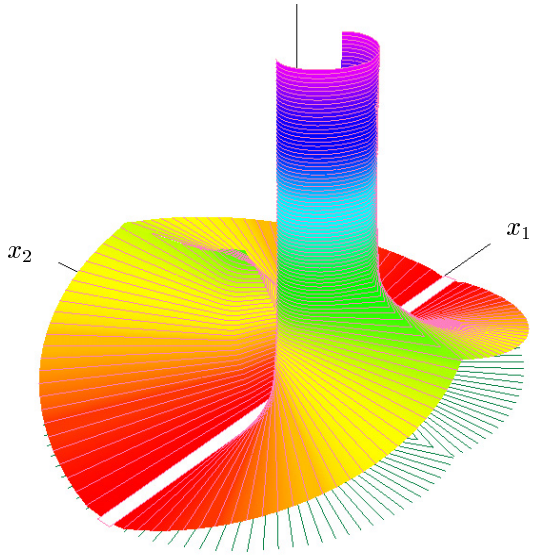

Fig. 54. The graph of the value function (with plotted level lines) for $w_e = 1.4$, $R = 0.3$ from another point of view.

6.3. *Level sets of the value function in the surveillance-evasion game*

In Figures 55–64, the computational results for $w^{(1)} = 1.7$ are presented. For all the figures except for Figures 63 and 64, the set Q is a regular hexagon inscribed into the unit circle with the center at the origin. The vertices are $(0,1)$, $(0.5,0.87)$, $(0.5,-0.87)$, $(0,-1)$, $(-0.5,-0.87)$ and $(-0.5,0.87)$. The half angle $\bar{\theta}$ of the detection cone is 45^0, 143^0, 136.3^0, 130^0, 125.6^0 and 121^0 for Figures 55, 56, 57a, 57b, 59a and 59b, respectively. According to the classification of the paper [19], Figures 55, 56, 57b and 59b correspond to the cases I, VI, V and IV. Figures 57a and 59a correspond to transient states. The step Δ is 0.01. Figure 55 shows the sets $W(\tau)$ for $\tau = 2\Delta i$, $i = \overline{1,65}$. In Figures 56, 57 and 59, the sets $W(\tau)$ for $\tau = 10\Delta i$, $i = \overline{1,k}$, are depicted ($k = 16, 18$ for Figures 56, 57a, and $k = 58$ for Figures 57b and 59). In this section, the boundaries of sets A and B are marked with dash lines.

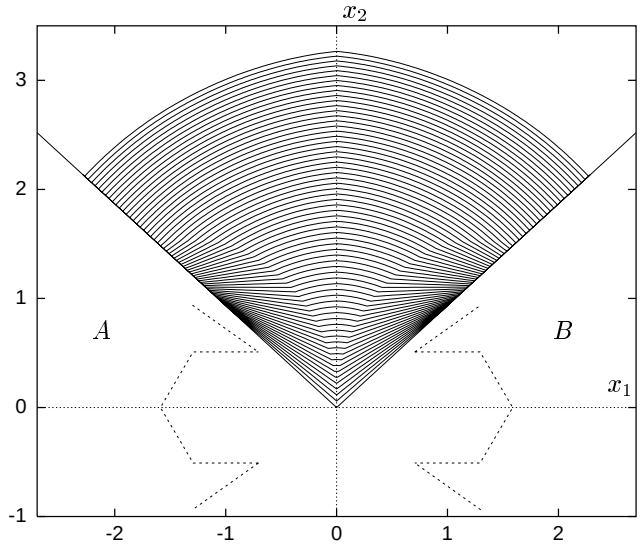

Fig. 55. Level sets of the value function of the surveillance-evasion game for $\bar{\theta} = 45^0$.

The player E escapes from all initial positions within the detection set given in Figure 55. The computations are done up to $\tau = 1.3$.

Figures 56, 57 and 59 show the gradual change of the escape zone with the decrease of the value $\bar{\theta}$. In Figures 57 and 59 the right half of each picture is only presented.

In Figure 56, the escape zone is bounded by two symmetric barrier lines abc and $a'b'c$ that emanate from the ends of the usable part and intersect at the point c. The maximal escaping time is $\tau = 1.6$.

The escape zone in Figure 57a is similar to that one in Figure 56. The barrier lines which bound the escape set touch the auxiliary sets A and B in the cusp points. The maximal escaping time is $\tau = 1.8$.

Further decrease in the value of $\bar{\theta}$ yields Figure 57b. The escape zone is bounded by the curve aef and symmetric to it curve $a'e'f$ with respect to the vertical axis.

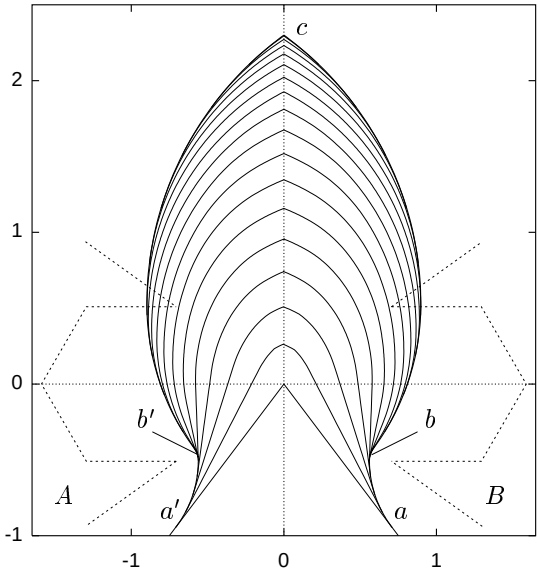

Fig. 56. Level sets of the value function of the surveillance-evasion game for $\bar{\theta} = 143^0$.

The arcs ae and $a'e'$ are parts of the barrier lines ab and $a'b'$ that finish on the boundary of auxiliary set B and A, respectively. The arc efe' is a limit of fronts as $\tau \to \infty$. Figure 58 shows a three-dimensional graph of the value function.

In Figure 59a, the boundary of the escape zone is also a limit of fronts as $\tau \to \infty$. Here, the point e (see Figure 57b) coincides with the point a.

Player E can escape from any point within the detection set in Figure 59b. The fronts go around the endpoint b of the barrier ab. After passing the point a, the end of the front moves down along the line $\theta = \bar{\theta}$ with a constant velocity. Thus the detection cone can be completely filled out with the fronts. As noted in [19], the escape zone coincides with the whole detection cone for cases similar to that shown in Figure 59b. The graph of the value function is given in Figure 60.

Note that the case shown in Figure 57a is a transient state from the situation where there is no accumulation of fronts (the escape set is similar to that one in Figure 56) to the situation where an accumulation of fronts occurs. The case shown in Figure 59a is a transient state from the case of the accumulation of fronts to the case where the detection cone is filled out with the fronts completely.

Figure 61 presents the fronts for a non-symmetric detection set. The left inclination angle corresponds to the case IV of the classification of [19], and the right one corresponds to the case VI. Figure 62 shows the graph of the value function.

The escape zone in Figure 63 is similar to that one in Figure 56 but a 25-polygon inscribed into the unit circle is used as the set Q instead of 6-polygon. The graph of the value function is given in Figure 64.

Let us compare the above solutions with those that can be obtained via solving the game of kind. When solving the game of kind, semipermeable curves are emitted

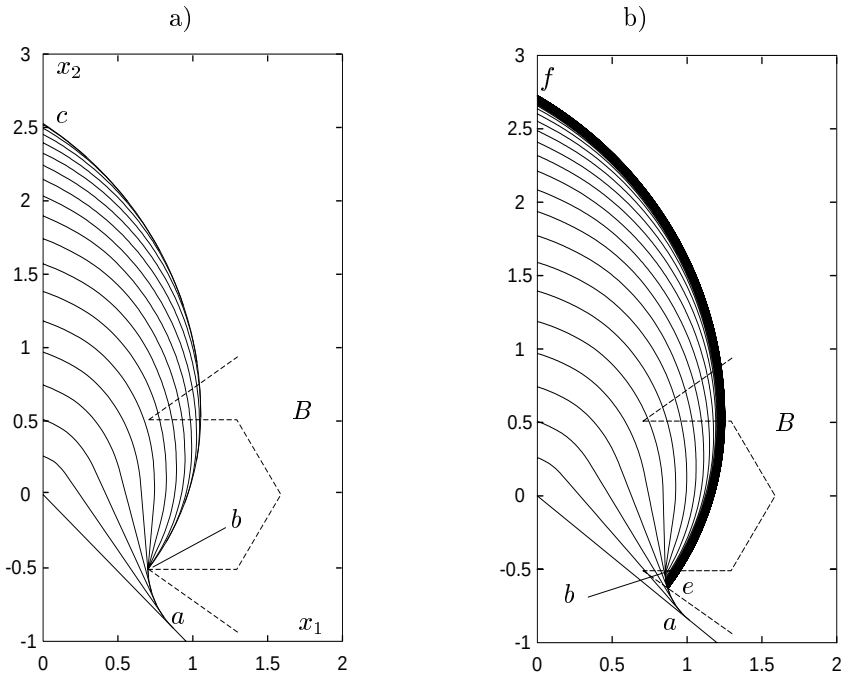

Fig. 57. The rise of accumulation of fronts; a: $\bar{\theta} = 136.3^0$ and b: $\bar{\theta} = 130^0$.

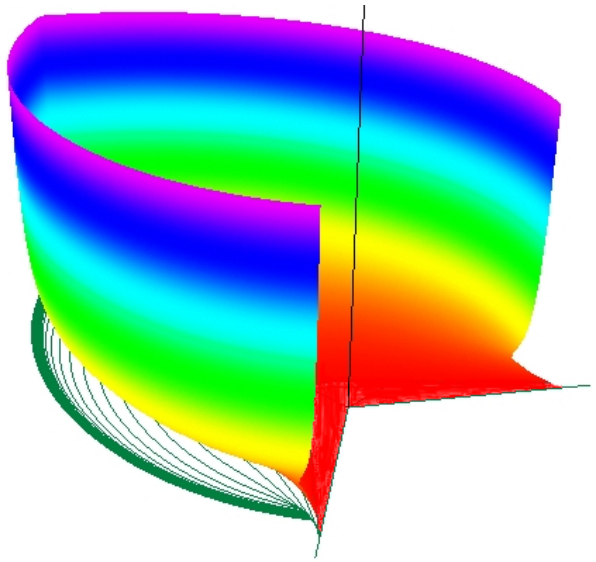

Fig. 58. The graph of the value function for level sets in Figure 57b.

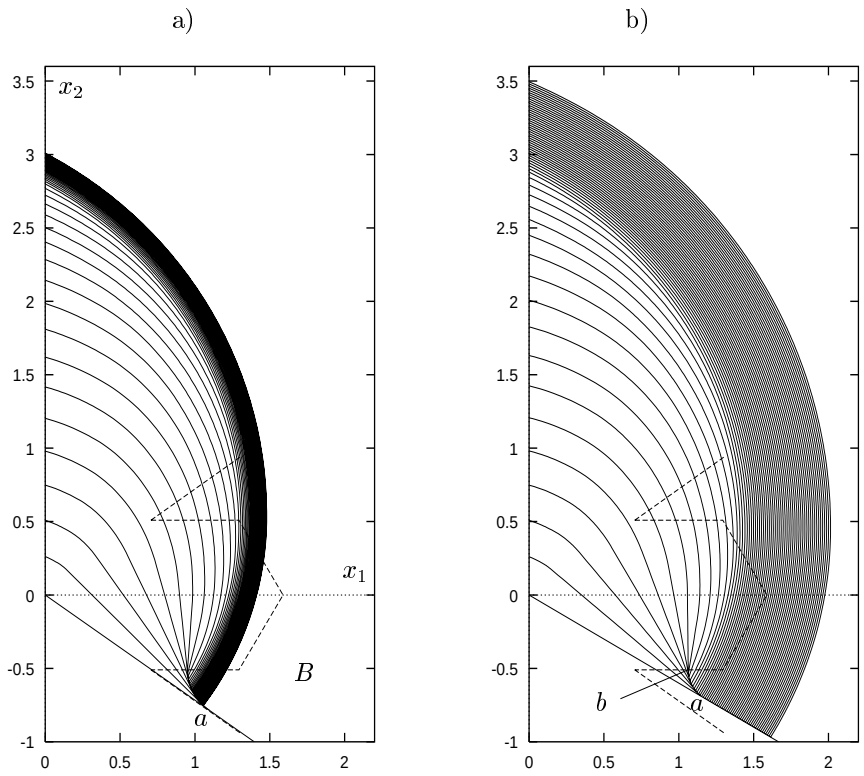

Fig. 59. The change of solution from a bounded to unbounded escape set; a: $\bar{\theta} = 125.6^0$ and b: $\bar{\theta} = 121^0$.

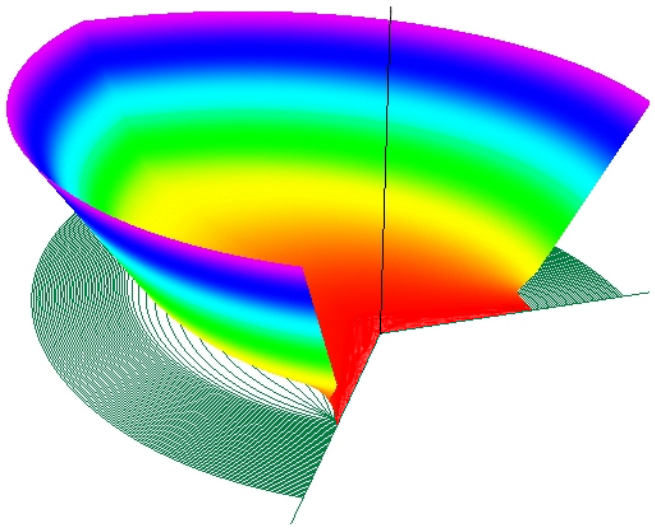

Fig. 60. The graph of the value function for level sets in Figure 59b.

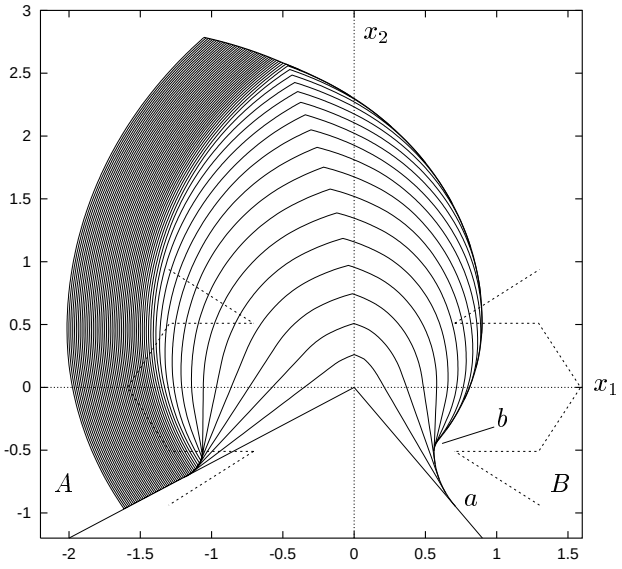

Fig. 61. Fronts for a non-symmetric detection cone.

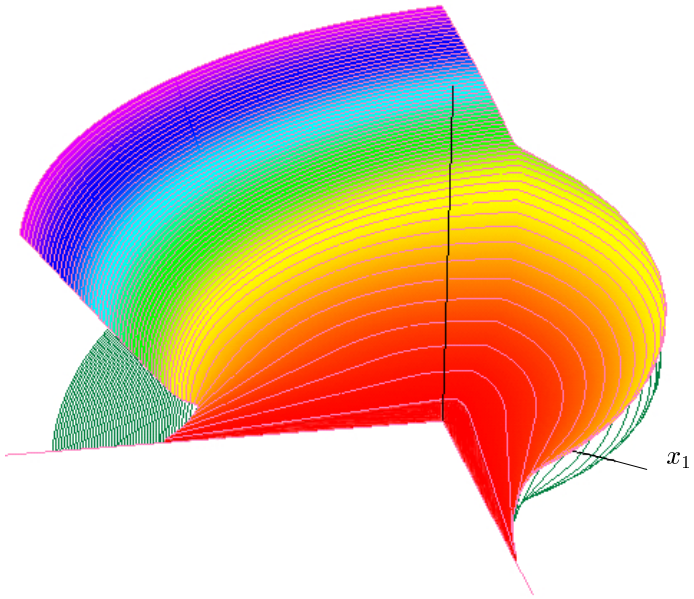

Fig. 62. The graph of the value function (with plotted level lines) for level sets in Figure 61.

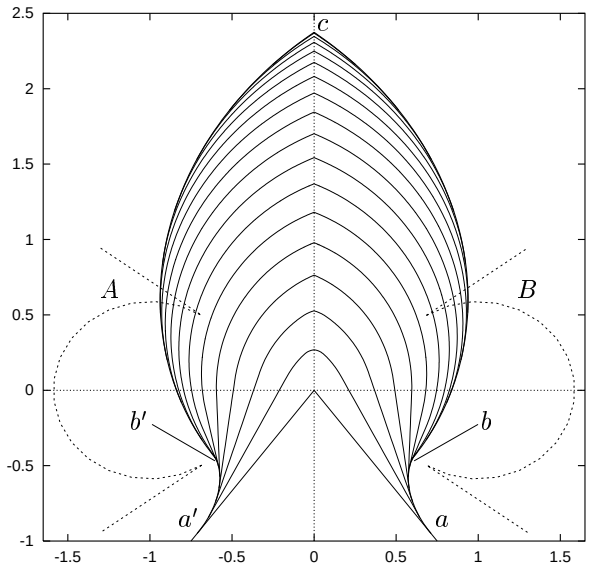

Fig. 63. Fronts for a circular constraint Q of player E.

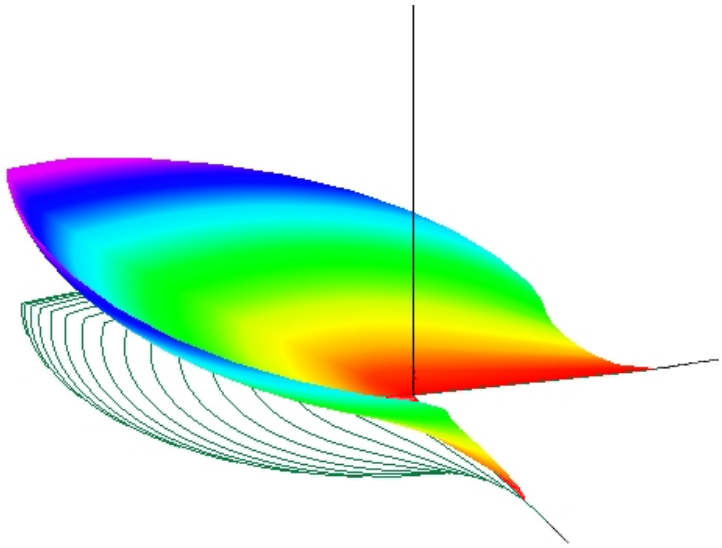

Fig. 64. The graph of the value function for level sets in Figure 63.

(see [21]–[23], [27] and [32]) in reverse time from endpoints of the usable part so that the semipermeability property (the property of barrier) holds at these points. In the game considered, the negative sides of the semipermeable curves emitted should be faced to the usable part. To provide this, a curve of the second type must emanate from the right endpoint of the usable part, and a curve of the first type must emanate from the left endpoint. The semipermeable curves with such properties are absent for the example in Figure 55. For the examples in Figures 56, 57, 59 and 63, the semipermeable curve $p^{(2),1}$ of the family $\Lambda^{(2),1}$ emanated in reverse time from the right endpoint a of the usable part is proper. The curve $p^{(2),1}$ is extended up to the boundary of the domain of $\Lambda^{(2),1}$. In Figures 56, 57, 59 and 63, the curve ab coincides practically with $p^{(2),1}$.

For the examples in Figures 56 and 63, the extended curve can be smoothly continued by a curve $p^{(2),2}$ of the family $\Lambda^{(2),2}$. After this continuation, a smooth composite semipermeable curve of the second type is obtained. Let us denote it by $g^{(2)}$. Because of the symmetry, there is a smooth composite semipermeable curve $g^{(1)}$ of the first type that emanates from the left endpoint a' of the usable part. The curves $g^{(2)}$ and $g^{(1)}$ intersect at a point that lies on the x_2-axis. This yields a composite barrier which bounds the solvability set of the game of kind (the escape set). The optimal guaranteed time of attaining the terminal set (escaping time) is finite for any initial point on the barrier. The above mentioned facts are completely confirmed by the computation of the fronts shown in Figures 56 and 63.

For the examples in Figures 57 and 59, the semipermeable curve $p^{(2),1}$ can not be smoothly continued beyond the endpoint. Moving along the curve $p^{(2),1}$ from the endpoint toward the point a, one looks for a point from which a semipermeable curve $p^{(2),2}$ of the family $\Lambda^{(2),2}$ emanates so that the composite curve $g^{(2)}$ formed by the initial part of $p^{(2),1}$ and the curve $p^{(2),2}$ would possess the semipermeability property at the sewing point. One can establish that such sewing points can only lie on the boundary of the domain of $\Lambda^{(2),2}$. A sewing point with the above property exists for the cases shown in Figures 57 and 59a.

Note that the sewing point in the case of Figure 57a coincides with the point b (therefore the curve $p^{(2),1}$ is completely included into the curve $g^{(2)}$), but the sewing point in the case of Figure 59a coincides with the point a (therefore no part of the curve $p^{(2),1}$ is included into the curve $g^{(2)}$). One can see that the point e is actually a sewing point in the case shown in Figure 57b. There are no sewing points for the case of Figure 59b.

The piecewise-smooth composite semipermeable curve $g^{(2)}$ and symmetric to it with respect to the x_2-axis curve $g^{(1)}$ define a solution to the game of kind in the cases corresponding to Figures 57 and 59a. Parts of these curves till the intersection point on the axis x_2 form a composite barrier that determines the solvability set of the game of kind. However in contrast to the examples in Figures 56 and 63, the escaping time in the cases of Figures 57b and 59a is infinite for any point that belongs to those parts of the composite barrier that are obtained using the curves $p^{(2),2}$ and $p^{(1),1}$. This nontrivial fact was mentioned in [19], and it is confirmed by the accumulation of fronts as $\tau \to \infty$ in Figures 57b and 59a.

In the case corresponding to Figure 59b, the solvability set of the game of kind coincides with the whole detection cone.

7. Conclusion

In the paper, differential games with dynamics of the homicidal chauffeur are studied numerically. Three variants of the problem setting are considered. Significant attention is paid to the analysis of families of semipermeable curves. This analysis is used for the verification of the computation of level sets of the value function, the computation being done with the algorithm developed by the authors. Examples that demonstrate the changes in solutions depending on the values of parameters of the problem are given. Solutions both with regions of accumulation of fronts and different variants of bending the barrier lines by the fronts are presented. The reality of multiply connected level sets of the value function is confirmed.

Acknowledgement. This research was partially supported by the Russian Foundation for Basic Researches under Grant No. 00-01-348.

References

[1] Aubin, J.-P. (1990). "A Survey of Viability Theory". *SIAM J. Control Optimization*, Vol. 28, No. 4, 749–788.

[2] Averbukh, V.L., S.S.Kumkov, V.S.Patsko, O.A.Pykhteev and D.A.Yurtaev (1999). "Specialized Vizualization Systems for Differential Games". In N.Mastorakis (ed.), *Progress in Simulation, Modeling, Analysis and Synthesis of Modern Electrical and Electronic Devices and Systems.* World Scientific and Engineering Society Press, 301–306.

[3] Bardi, M. and M.Falcone (1990). "An Approximation Scheme for the Minimum Time Function". *SIAM J. Control Optimization*, Vol. 28, 950–965.

[4] Bardi, M., M.Falcone and P.Soravia (1997). "Numerical Methods for Pursuit-Evasion Games via Viscosity Solutions". Preprint No. 38, Universita degli di Roma "La Sapienza", Dipartimento di Matematica "Guido Castelnuovo".

[5] Bardi, M., M.Falcone and P.Soravia (1999). "Numerical Methods for Pursuit-Evasion Games via Viscosity Solutions". In M.Bardi, T.E.S.Raghavan, and T.Parthasarathy (eds.), *Stochastic and Differential Games: Theory and Numerical Methods, Annals of the International Society of Dynamic Games.* Boston: Birkhäuser, Vol. 4, 105–175.

[6] Bernhard, P. (1971). "Conditions de Coin Pour les Jeux Differentiels". Seminaire sur les Jeux Differentiels, Centre D'Automatique, Paris.

[7] Bernhard, P. and B.Larrouturou (1989). "Etude de la barriere pour un probleme de fuite optimale dans le plan". Rapport de Recherche, INRIA, Sophia-Antipolis.

[8] Breakwell, J.V. (1977). "Zero-Sum Differential Games with Terminal Payoff". In P.Hagedorn, H.W.Knobloch, and G.J.Olsder (eds.), *Differential Games and Applications. Lecture Notes in Control and Information Sciences.* Berlin: Springer-Verlag, 70–95.

[9] Cardaliaguet, P., M.Quincampoix and P.Saint-Pierre (1994). "Some Algorithms for Differential Games with Two Players and one Target". *RAIRO-Modelisation-Matematique-et-Analyse-Numerique*, Vol. 28, No. 4, 441–461.

[10] Cardaliaguet, P., M.Quincampoix and P.Saint-Pierre (1995). "Numerical Methods for Optimal Control and Differential Games". Ceremade CNRS URA 749, University of Paris-Dauphine.

[11] Cardaliaguet, P. (1997). "Nonsmooth Semipermeable Barriers, Isaacs' Equation, and Application to a Differential Game with One Target and Two Players". *Applied Mathematics and Optimization*, Vol. 36, 125–146.

[12] Cardaliaguet, P., M.Quincampoix and P.Saint-Pierre (1999). "Set-Valued Numerical Analysis for Optimal Control and Differential Games". In M.Bardi, T.E.S.Raghavan, and T.Parthasarathy (eds.), *Stochastic and Differential Games: Theory and Numerical Methods, Annals of the International Society of Dynamic Games.* Boston: Birkhäuser, Vol. 4, 177–247.

[13] Grigor'eva S.V., A.M.Taras'ev, V.N.Ushakov and A.A.Uspenskii (1996). "Constructions of Nonsmooth Analysis in Numerical Methods for Solving Hamilton-Jacobi Equations". *Nova J. Math. Game Theory Algebra*, Vol. 6, No. 1, 27–44.

[14] Ivanov, V.A., A.M.Taras'yev, V.N.Ushakov and A.P.Khripunov (1993). "The Toreador Problem". *J. Appl. Math. Mech.*, Vol. 57, No. 3, 419–425.

[15] Isaacs, R. (1965). *Differential Games.* New York: John Wiley.

[16] Krasovskii, N.N. and A.I.Subbotin (1974). *Positional Differential Games.* Moscow: Nauka (in Russian).

[17] Krasovskii, N.N. and A.I.Subbotin (1988). *Game-Theoretical Control Problems.* New York: Springer-Verlag.

[18] Lewin, J. and J.V.Breakwell (1975). "The Surveillance-Evasion Game of Degree". *Journal of Optimization Theory and Applications*, Vol. 16, No. 3-4, 339–353.

[19] Lewin, J. and G.J.Olsder (1979). "Conic Surveillance Evasion". *Journal of Optimization Theory and Applications*, Vol. 27, No. 1, 107–125.

[20] Merz, A.W. (1971). *The Homicidal Chauffeur – a Differential Game*, PhD Dissertation, Stanford University.

[21] Patsko, V.S. (1973). *Problem of Kind in Linear Differential Games of the Second Order*, PhD Dissertation, Ural State University, Sverdlovsk (in Russian).

[22] Patsko, V.S. (1975). "The Problem of Quality in Second Order Linear Differential Games". In A.B.Kurzhanskii (ed.), *Differential Games and Control Problems.* Sverdlovsk: Institute of Mathematics and Mechanics, 167–227 (in Russian).

[23] Patsko, V.S. and V.L.Turova (1995). "Numerical Solution of Two-Dimensional Differential Games". Preprint of the Institute of Mathematics and Mechanics, Ekaterinburg.

[24] Patsko, V.S. and V.L.Turova (1996). "Minimum-Time Problem for Linear Second-Order Conflict-Controlled Systems". *Proceedings of UKACC International Conference on CONTROL'96*, Exeter, United Kingdom, 947–952.

[25] Patsko, V.S. and V.L.Turova (1997). "Numerical Solutions to the Minimum-Time Problem for Linear Second-Order Conflict-Controlled Systems". *Proceedings of the Seventh International Colloquium on Differential Equations*, Plovdiv, Bulgaria, 327–338.

[26] Raivio, T. and H.Ehtamo (1998). "On Numerical Solution of a Class of Pursuit-Evasion Games", Helsinki University of Technology (manuscript).

[27] Subbotin, A.I. and V.S.Patsko (eds.) (1984). *Algorithms and Programs for Solving Linear Differential Games*. Sverdlovsk: Institute of Mathematics and Mechanics (in Russian).

[28] Subbotin, A.I. (1995). *Generalized Solutions of First-Order PDEs: the Dynamical Optimization Perspective*. Boston: Birkhäuser.

[29] Subbotin, A.I. (1999). "Constructive Theory of Positional Differential Games and Generalized Solutions to Hamilton–Jacobi Equations". In M.Bardi, T.E.S.Raghavan, and T.Parthasarathy (eds.), *Stochastic and Differential Games: Theory and Numerical Methods, Annals of the International Society of Dynamic Games*, Vol. 4, Boston: Birkhäuser, 3–67.

[30] Taras'yev, A.M., V.N.Ushakov and A.P.Khripunov (1987). "On a Computational Algorithm of Solving Game Control Problems". *J. Appl. Math. Mech.*, Vol. 51, No. 2, 167–172.

[31] Tarasyev, A.M., V.N.Ushakov and A.P.Khripunov (1992). "On a Numerical Algorithm for Solving Game-Theoretical Problems of Control". *Trudy Instit. Matem. Mekh. UrO RAN*, Vol. 1, 160–177 (in Russian).

[32] Turova, V.L. (1985). "Nonlinear Differential Game of Kind in the Plane". In A.I.Subbotin and V.S.Patsko (eds.), *Investigations of Minimax Control Problems*, Sverdlovsk: Institute of Mathematics and Mechanics, 91–116 (in Russian).

[33] Ushakov, V.N. (1981). "On the Problem of Constructing Stable Bridges in a Differential Game of Approach and Avoidance". *Engrg. Cybernetics*, Vol. 18, No. 4, 16–23.

[34] Ushakov, V.N. (1998). "Construction of Solutions in Differential Games of Pursuit-Evasion". *Differential Inclusions and Optimal Control. Lecture Notes in Nonlinear Analysis*, Vol. 2, Nicholas Copernics University, Torun, 269–281.

Valeri Semenovich Patsko
Varvara Leonidovna Turova

Numerical study of differential games with the homicidal chauffeur dynamics

Scientific reports

Institute of Mathematics and Mechanics, UrB of RAS.
620219, Russia, Ekaterinburg, GSP-384,
S.Kovalevskaya str. 16.